THREE STAGE POTASSIUM

TEST TURBINE

FINAL DESIGN - VOLUME I - FLUID DESIGN

By

R. J. Rossbach

G. C. Wesling

W. F. Lemond

prepared for

NATIONAL AERONAUTICS AND SPACE ADMINISTRATION

CONTRACT NAS 3-8520

SPACE POWER AND PROPULSION SECTION

MISSILE AND SPACE DIVISION

GENERAL ELECTRIC

CINCINNATI, OHIO 45215

Requests for copies of this report
should be referred to:

National Aeronautics & Space Administration
21000 Brookpark Road
Cleveland, Ohio 44135
Attn: Contracting Officer
      Space Power Systems Procurement Section
      MS 500-309

THE DESIGN OF A THREE-STAGE POTASSIUM TURBINE -

VOLUME I - FLUID DESIGN

by

R.J. Rossbach
G.C. Wesling
W.F. Lemond

TABLE OF CONTENTS

SUMMARY

A three-stage potassium vapor turbine has been designed for testing in the existing 3000 KW facility with 1550°F inlet vapor temperature. The turbine is designed for 15,000 hours operation with eight to ten percent liquid entering the third stage which has a tip speed of 835 ft./sec. This turbine is a growth version of the successful two-stage potassium turbine and is based on the same design principles. The additional stage and more extensive instrumentation are expected to provide better understanding of wet potassium vapor turbines.

INTRODUCTION

In Rankine-cycle space power systems, operating on potassium vapor, some or all of the turbine stages are expected to operate in the wet vapor region for 15,000 hours or more. Suitable blading materials must be found which are both compatible with potassium vapor and resistant to droplet impact erosion. Besides blade material properties, the rate of impact erosion is known from steam turbine practice to increase with tip speed and moisture content.

A two-stage potassium turbine (1)[*] was designed, built and tested under NASA Contract NAS 5-1143. This turbine had about four percent liquid entering the second stage which had a tip speed of 770 ft./sec. at the endurance test conditions. After 5000 hours of testing at these conditions, there was no evidence of impact erosion on the TZM refractory alloy blades. However, it is desirable to design potassium-turbine stages for operation at higher values of moisture fraction and tip speed than the aforementioned values.

As a result, the Re-Entry Systems Department of the General Electric Company has been under contract to the National Aeronautics and Space Administration since July 5, 1966 for the design, fabrication and assembly of a three-stage test turbine suitable for operation in wet potassium vapor at 1550°F turbine inlet temperature. The main objectives of this program are the attainment of wet vapor, with a moisture fraction of eight to ten percent entering the third stage at a tip speed of 835 ft./sec. and a turbine life of 15,000 hours. The three-stage turbine is designed for installation and test in the existing 3000 KW facility.

---

[*] Numbers in parentheses indicate references listed in this report.

DESIGN CONSIDERATIONS

The design procedures used for the three-stage turbine were developed through experience on the two-stage potassium turbine program under Contract NAS 5-1143. The basic assumption is that wet potassium vapor expands through the nozzle and rotor blade rows of each stage in a supersaturated condition and then reverts to equilibrium conditions at the exit of each rotor blade row. Calculations based on this model gave predicted turbine performance that was verified by performance measurements during testing of the two-stage potassium turbine (2).

This model permits the use of gas turbine calculation programs for the supersaturated vapor expansion through each stage. At the exit of each stage a calculation is made to determine the conditions after reversion from super-saturated to equilibrium conditions. This calculation satisfies the conservation equations of mass, energy and momentum for the supersaturated and equilibrium states. The important results of the reversion calculation are that some of the vapor is condensed, and the vapor temperature rises to its equilibrium value; the equilibrium values are used as input for the next stage.

A performance loss due to the droplet drag of the condensed liquid is based on the energy expended by the rotor in accelerating the moisture which enters a stage up to the mean wheel speed of the stage.

The first step in the design of the three-stage turbine was the design of the first two stages to produce 8 to 10 percent moisture. Shown in Figure 1 is a sketch of a turbine expansion process on the potassium Mollier

diagram. It can be seen that in order to achieve wet vapor with 8 to 10 percent moisture it is necessary to extract about 80 Btu of energy from each pound of vapor. To accomplish this in two stages which can be tested in the existing 3000 KW facility required blade turning angles very similar to those of the two-stage turbine developed and tested under NASA Contract NAS 5-1143. An optimization study indicated that the best turbine configuration for these conditions had an efficiency less than one percent higher than that of the two-stage potassium turbine. Therefore, the first two stages of the three-stage turbine will have the same blading as the two-stage turbine developed under the NASA 5-1143 contract.

The turbine expansion shown in Figure 1 was calculated for the three-stage turbine operating at 1550°F inlet vapor temperature and 18,250 rpm, which are the design conditions for the endurance test. Because a super-saturated expansion process cannot be shown properly on a Mollier diagram which represents equilibrium state points, the equilibrium points at the inlet and exit of each stage are connected by dashed lines. The first stage expansion is from a total pressure of 30.86 psia to a static pressure of 15.7 psia, the second stage expansion is from a total pressure of 16.8 psia to a static pressure of 7.66 psia, and the third stage from 8.65 to 3.71 psia. The intermediate pressures shown for each stage are the total pressure relative to the rotating blade and the static pressure at the nozzle exit station.

A pitchline design point calculation program was used for preliminary design of the third stage. The stage was designed for the exit flow and pressure conditions of the two-stage turbine operating at 18,250 rpm, with

inlet vapor temperature of 1500°F and a total-to-total pressure ratio of 3.4. The pressure ratio is high enough to provide the maximum amount of moisture that can be obtained with the two-stage turbine. The rotative speed is the design value. The inlet vapor temperature was chosen midway between the operating limits of 1450 to 1550°F. Performance calculations for the two-stage turbine indicate that turbine efficiency is not sensitive to variations of inlet temperature in this range. The third stage annulus flow area was made about 42 percent larger than that of the second stage. This is a reasonable area expansion consistent with the first two stages. The design parameters that were varied for the third stage were nozzle flow angle, nozzle exit velocity and stage work. For each value of nozzle angle there is one value of nozzle exit velocity that will satisfy the requirements of flow rate and annulus area. The stage work determines the blade turning and exit swirl. A stage with a nozzle flow angle of 68 degrees from axial and a stage work of 40 Btu/lb. was selected. This stage loading is consistent with the first two stages which are heavily loaded in order to get the maximum amount of condensed liquid at the exit of the second stage.

A lightly loaded third stage was considered for increased turbine efficiency. A stage with a nozzle angle of 66 degrees and stage work of 30 Btu/lb. had a calculated stage efficiency five percent higher than the one selected. However, the substitution of this lightly loaded third stage increased the efficiency of the three-stage turbine less than one percent. The more heavily loaded stage was selected as representative of a realistic turbine design. The prime requirement for this application is the attainment of high moisture content which can only be done in two stages by having them heavily loaded.

A three-stage turbine designed for maximum efficiency would have three lightly loaded stages and less condensed liquid.

The effect of rotor tip shrouds was investigated as a way to improve turbine efficiency. Shrouds reduce tip clearance loss partly due to less interference between the leakage flow and the mainstream flow and partly due to the fact that the more tortuous path which the flow must take over the shroud will reduce the actual quantity of leakage flow. Ainley and Mathieson (3) suggest that the clearance loss for a shrouded blade row is about half of the clearance loss for an unshrouded blade row with the same tip clearance. Applying this suggestion to the calculation of stage efficiency for the three-stage turbine indicates that the use of tip shrouds would improve the efficiencies by 4, 3 and 2 percent for the respective stages. The effect is greatest for the first stage because the blade height is least and therefore the percentage tip clearance and loss is greatest. The calculated improvement in overall turbine efficiency due to tip shrouds is about three percent.

Shown in Figure 2 is the variation of turbine efficiency with total-to-static pressure ratio. The actual turbine work is based on supersaturated expansion of the vapor. For the two upper lines no reversions were assumed and the ideal turbine work is based on supersaturated conditions; the top line is for an ideal condition of zero tip clearance and the middle line shows the performance penalty associated with the design values of tip clearance with rotor tip shrouds. The lowest line is based on reversions to equilibrium conditions after each rotor blade row with the ideal turbine work based on potassium equilibrium properties. It can be seen that there is a significant difference

in turbine efficiency when an ideal equilibrium expansion is used as the basis.
For example, the turbine efficiency at a total-to-static pressure ratio of 8.0
is 119/142 or 0.838 for the supersaturated calculation and 114/161 or 0.708
based on equilibrium conditions. The lower numerator of the equilibrium case
reflects the losses due to condensation and droplet drag. The larger denomina-
tor reflects the greater ideal expansion energy of the equilibrium process
across a given pressure ratio.

Shown in Figure 3 is a layout drawing of the three-stage turbine flow
path in the hot condition with tip shrouds on all three stages. The use of
tip shrouds creates a potential problem in that liquid may collect in the
tip seal cavity if the cavity is not drained. It is not desirable to drain
these cavities for the initial assembly because high moisture content at the
third stage is one of the program objectives. Downstream of each rotating
blade row the flow annulus was increased at the tip to prevent the buildup
of condensed potassium liquid in the rotating tip seal. To determine any
performance penalty that might be incurred, the sudden expansion loss was
estimated behind each rotating blade row using compressible flow theory.
For expansion area ratios from 15 to 10 percent and Mach numbers from 0.25
to 0.4, the sudden expansion pressure loss was from 2 to 1 percent of the
velocity head. It was estimated that these sudden expansion losses would
cause a negligible 0.2 percent loss in turbine efficiency.

AERODYNAMIC DESIGN

In the design of potassium turbines for operation in the wet vapor region, the basic assumption is that the vapor expands through each stage in a supersaturated condition with reversion to equilibrium after each rotor. The values of the polytropic exponent for supersaturated expansion were determined by flow through a nozzle under the NAS 5-1143 contract (4). The potassium properties used are those of NRL Report 6233 (5) by the U.S. Naval Research Laboratory.

A detailed fluid design of the third stage has been carried out using an axisymmetric flow determinations computer program. This program was used to calculate flow velocities and angles at eleven streamlines and five axial locations, by solving the equations of energy, continuity and radial equilibrium, includingthe effects of streamline slope and curvature. Inputs to this program are flowpath dimensions, rotative speed, inlet pressure and temperature, flow rate, energy of the fluid entering and leaving the rotor, and efficiency of each blade row.

Shown in Figure 4 are plots of axial velocity as a function of radius at four axial locations in the third stage. The distributions for the nozzle exit and bucket inlet have a negative slope due to the concave inward curvatures of the streamlines at the tip. The axial velocity distributions for the bucket and stage exit have a positive slope because of convex inward curvature near the tip. The differences in axial velocity between nozzle exit and bucket inlet and between bucket and stage exit are due to changes in curvature and losses between the blade rows.

Shown in Figure 5 is the radial variation in vapor flow angles at four
axial locations in the third stage. These angles are measured from axial and
positive values are in the direction of rotation. The bucket and stage exit
values are negative and the flow angles at bucket inlet and exit are relative
to the rotating wheel. The bucket turning angle varies from 77 degrees at the
tip to 109 degrees at the hub. At the hub the bucket exit angle is greater
than the bucket inlet angle, indicating accelerating flow or positive reaction.
The maximum nozzle efflux angle is 72.5 degrees at the tip; high values of
nozzle efflux angle were used to reduce the axial velocity level through the
stage.

Shown in Figure 6 is the radial variation of reaction for the third stage.
Reaction is defined as the ideal static enthalpy drop across the rotor divided
by the ideal total-to-static enthalpy drop across the stage. Since the aero-
dynamic calculations were made with a gas turbine program assuming supersaturated
vapor expansion the formula is

$$R_x = \frac{P_{s1}^{\frac{\gamma-1}{\gamma}} - P_{s2}^{\frac{\gamma-1}{\gamma}}}{P_{t0}^{\frac{\gamma-1}{\gamma}} - P_{s2}^{\frac{\gamma-1}{\gamma}}}$$

where

P_{t0} is total pressure at stage inlet.

P_{s1} is static pressure after nozzle.

P_{s2} is static pressure after rotor.

γ is polytropic exponent for expansion.

R_x is reaction.

The reaction varies from 16 percent at the hub to 48 percent at the tip. The fairly high reaction was chosen to improve the stage efficiency. The radial variation of Mach number is shown in Figure 7. The Mach numbers are subsonic in all cases indicating that the turbine is unchoked. The stage exit Mach number is around 0.4, which is slightly greater than the exit Mach numbers in the first two stages.

Shown in Figure 8 are the velocity vector diagrams for the third stage from the aerodynamic design program. These diagrams were drawn using the velocities and flow angles for the bucket inlet and exit locations and the wheel speeds for 18,250 rpm. The results from the Turbine Flow Determinations program were used to design the nozzle vanes and rotor blades for the third stage.

The design of the first two stages was discussed in reports issued under Contract NAS 5-1143 and in Reference 1. The design conditions were 1600°F inlet vapor temperature and 19,200 rpm. The first set of hardware for the two-stage turbine had a first stage nozzle effective flow area about 10 percent larger than design. This caused a shift of turbine work from the first to the second stage with a reduction of about one percent in turbine efficiency. For the second set of hardware the first stage nozzle vanes were turned about two degrees to reduce the nozzle passage throat width. Off-design calculations for the two-stage turbine indicate that the second configuration had 1 1/2 percent higher total-to-total efficiency and 3 1/2 percent better total-to-static efficiency than the first one. This second configuration was used for the first two stages of the three stage turbine. Shown in Figure 9 are mean line velocity vector diagrams for the three turbine stages as calculated with the off-design program at 18,250 rpm, 1550°F inlet vapor temperature and a turbine inlet total-to-exit static pressure ratio of 8.3.

BLADING DESIGN

The objective is to design blades that will produce the flow conditions specified by the results of the axisymmetric Turbine Flow Determinations program. The nozzle vane chord was chosen as one inch which is consistent with the first two stages and results in a Reynolds number of 1.8×10^5 at the design condition. The rotor blade chord was chosen at 0.85 inch with a Reynolds number of 1.0×10^5. The number of nozzle vanes was chosen at 44, for a solidity of 1.51 at the pitch diameter. The selection of 52 buckets for the third stage rotor results in a solidity of 1.51. These values of solidity are slightly greater than recommended in reference 3, but are consistent with General Electric Co. practice.

Using 44 nozzle vanes the throat dimension for the nozzle passages was calculated as a function of radius; $d_o = \frac{2\pi r}{n} \cos \alpha$, where d_o is nozzle throat width, $\frac{2\pi r}{n}$ is tangential spacing, and α is efflux flow angle from axial. This throat dimension is shown by the solid lines in Figure 10. The points indicated by circles are the values selected for the design and they deviate from the calculated values in the tip region. This deviation results from the requirement of linear twist of the nozzle vanes and is acceptable because of uncertainties in the streamline curvature and aerodynamic losses in the tip region. Using the appropriate throat dimensions and tangential spacing, nozzle blade shapes were drawn for the pitch, tip and hub sections. The selected blade profile oriented for the pitch radius is shown in Figure 11. The blade has a constant cross-section and only the orientation angle varies with the radius. The blade coordinates, listed in Table I, were input to a cascade analysis program which solves for the velocity distribution around a blade profile in

cascade, based on incompressible, two-dimensional flow. Shown in Figures 12, 13 and 14 are the velocity distributions for the nozzle vanes at hub, pitch and tip sections at the design inlet angle and appropriate orientation angles. The ordinate is the ratio of blade surface velocity to stream exit velocity and the abscissa is axial distance from the trailing edge of the nozzle vane. The upper line is for the suction or convex side of the vane and the lower line is for the pressure or concave side. A major criterion for acceptance of a blade profile is that the maximum velocity ratio should be less than 1.15 to minimize diffusion. It can be seen from these plots that this criterion is satisfied.

The blade sections for the rotor were designed in a similar manner. Using 52 blades, with a solidity of 1.51 at the mean radius, and the results of the axisymmetric flow program the throat dimension for the rotor blade passages was calculated as a function of radius; $d_o = \dfrac{2\pi r}{n} \cos \beta$, where d_o is rotor passage throat width, $\dfrac{2\pi r}{n}$ is tangential spacing, and β is exit flow angle relative to blade. This throat dimension is shown by the solid lines in Figure 15. Using the appropriate throat dimensions, indicated by the circles in Figure 15, and tangential spacing, rotor blade shapes were drawn for five radial stations in the flow annulus. Shown in Figures 16, 17 and 18 are the blade shapes at the hub, mean and tip sections. The blade coordinates, listed in Table II, were input to the cascade analysis program. Based on the results from the program, the blade shapes were modified until the ratio of surface velocity to stream exit velocity was smooth with a minimum amount of diffusion from the throat to the blade trailing edge. Shown in Figures 19, 20 and 21 are the velocity ratio plots for the hub, mean and tip sections at design inlet conditions. The velocity ratio was a maximum of 1.225 for the suction or convex surface of the hub blade section and less

for the other blade sections. Although this velocity ratio is slightly greater than it was for the nozzles, the stream exit velocity is generally lower for the rotor blades and a higher velocity ratio is considered satisfactory.

TURBINE EXIT SYSTEM

The turbine exit system, shown in Figure 22, consists of the diffuser, the collector or scroll, and the transition section into the ten inch diameter pipe leading to the condenser. The exit diffuser is designed to reduce the turbine exit velocity and recover a portion of the velocity head as an increase in static pressure. The diffuser portion of the exit system was designed at a turbine total-to-static pressure ratio of 6.98. At this condition the turbine exit velocity is very nearly axial. Several different diffuser configurations were analyzed using a subsonic, compressible flow analysis. The main objective of the analysis was to obtain a diffuser configuration which would have no high diffusion rates on either surface to minimize the possibility of boundary layer separation on either surface. The final configuration chosen is the one shown in Figure 22. Shown in Figures 23 and 24 are the diffuser passage width and area which gives the diffuser an area ratio of 2.19. The results of the diffuser flow analysis are shown in Figure 25 as surface Mach number along the upper and lower surfaces. Because of the static pressure recovery in the diffuser, the total-to-static turbine efficiency obtained from measurements at the diffuser exit should be approximately 2.5 percent higher than that obtained from measurements at the turbine exit at the match point.

At the diffuser exit, the flow is dumped into a collector or scroll passage to be carried tangentially around the turbine to the ten-inch diameter pipe into the condenser. Twelve one-half inch diameter struts required for mechanical strength have been located at the diffuser exit in lieu of vanes

near the diffuser inlet in order to not separate the flow in the diffuser.
These rods cause an area blockage of about 12 percent at the diffuser exit.
After the diffuser exit, baffles are placed parallel to the diffuser walls
to prevent recirculation of the flow across the top of the diffuser.

The collector portion of the exhaust system is symmetric about the tur-
bine centerline down to the transition section. The transition section is
confined to a relatively small space because of the physical dimensions of
the test facility. The resulting transition section is an attempt to have
a flow passage which will carry the flow from the collector into the ten-inch
pipe in a relatively efficient manner and which is relatively simple and
inexpensive to manufacture.

INSTRUMENTATION

Instrumentation will be improved over that used on the two-stage turbine. Additional thermocouples will be used between each blade row to measure interstage temperatures. Temperatures and pressures will be measured at turbine inlet and exit stations to determine overall performance, and between each blade row to determine stage performance. Additional pressure and temperature measurements will be made in the exit diffuser and scroll.

The efflux pressure measurement system will be utilized to measure pressures at all stations including the bulletnose differential pressure measurements which are used to determine the vapor flow rate. Inlet vapor quality will be determined using the throttling calorimeter. Turbine torque will be measured with Bytrex strain gage torquemeters. All measurements will be recorded through the digital readout system. Exit quality will be determined by means of an energy balance. The turbine enthalpy change is calculated from measurements of turbine torque, rotative speed and vapor flow rate. The turbine exit quality is then calculated from exit enthalpy and exit total pressure.

The performance instrumentation are listed in Table III, including the parameter to be measured, the circumferential location of the sensor at each measurement station, the range of measurement and the sensor. The instrumentation stations are shown in Figure 22.

All thermocouples will be calibrated before installation in the turbine. They will be checked at three temperature levels using the freezing points of zinc, 787.1°F, aluminum, 1220°F, and silver 1761.4°F. The efflux system

pressures will be connected to five scanner switches. Each scanner has one pressure transducer. These transducers will be individually calibrated by varying the pressure level from 0 to 50 psia and comparing digital readout of the transducers with a Wallace and Tierman Model FA129 0-50 psia pressure indicator. The Wallace and Tierman gage is periodically checked against a C.E.C. Pressure Standard which is traceable to the National Bureau of Standards.

OFF-DESIGN PERFORMANCE

Preliminary off-design performance has been calculated for the three-stage turbine. Shown in Figure 26 is the variation of vapor flow rate with turbine inlet total-to-exit static pressure ratio for operation at 18,250 rpm with vapor inlet temperature of 1500°F. The vapor flow rate is constant at turbine pressure ratios greater than 8. Shown in Figure 27 is the variation in turbine power output for the same conditions. The power increases up to a pressure ratio of about 12, with only slight increases at greater pressure ratios as the turbine becomes choked. The variation in turbine efficiency is shown in Figure 28. Although the total-to-total efficiency is practically constant, the total-to-static efficiency decreases at the high pressure ratios due to the greater leaving loss associated with the higher exit velocities. These efficiency values were calculated for shrouded rotor blades with the hot tip clearances, and are based on the total and static pressures at the exit of the third stage. A turbine efficiency based on the static pressure in the exit scroll would be midway between the static and total efficiencies shown. This is because half of the dynamic head can be recovered by the diffuser and exit system; the remainder is lost due to total pressure losses in the diffuser and scroll.

Shown in Figure 29 is the variation in vapor quality at the entrance to the second and third stages, based on a turbine inlet quality of 0.99. At a total-to-static pressure ratio of 8.0 the quality is 0.944 into the second stage and 0.903 into the third stage.

Similarly, the performance of the three-stage turbine was calculated at vapor inlet temperatures of 1450 and 1550°F and is shown in Figures 30 through 39. These plots show the same characteristics seen in the 1500°F plots. The variation in performance with rotative speed is seen to be small from 15,400 to 20,000 rpm. Note that the second stage exit quality at 1550°F inlet temperature is 0.901 at a pressure ratio of 7.9, which is the endurance test condition.

CONCLUDING REMARKS

A three-stage potassium vapor turbine has been designed as part of the NASA Rankine Systems Technology Program. A major objective is to determine whether there is an erosion problem associated with the greater quantity of condensed liquid and higher tip speeds of the third stage. This turbine is a growth version of the successful two-stage potassium turbine and is based on the same design principles. The first two stages are unchanged aerodynamically except that rotor tip shrouds have been added to reduce tip clearance loss and increase efficiency. The third stage has been designed to match the first two stages at a condition where the vapor quality out of the first two stages is about 91 percent. The aerodynamic analysis and blade designs are based on General Electric Co. design programs as were the first two stages.

Another objective of the three-stage turbine program is to gain a better understanding of two phase potassium expansion processes. The assumption of supersaturated vapor expansion in each stage with reversion to equilibrium after each rotor blade row seemed to be verified by the test results of the two-stage turbine. However, the additional stage and more extensive instrumentation are expected to provide better understanding of wet potassium vapor turbines.

REFERENCES

1. Space-Vehicle Rankine-Cycle Power Plant Potassium-Turbine Development, R.J. Rossbach, ASME 63-WA-326, Nov. 1963.

2. Performance Test of a Two Stage, 200 HP Turbine in Wet Potassium Vapor, R.J. Rossbach, E. Schnetzer, H.E. Nichols, S.E. Eckard, AIAA Specialists Conference on Rankine Space Power Systems, Vol. 1, CONF-651026, Oct. 1965.

3. A Method of Performance Estimation for Axial Flow Turbines, D.G. Ainley and G.C.R. Mathieson, A.R.C. (British) R. and M. No. 2074, Dec. 1951.

4. Critical Flow of Potassium Vapor Through Instrumented Converging-Diverging Nozzle, R.J. Rossbach, ASME 65-GTP-22, March, 1965.

5. High-Temperature Properties of Potassium, C.T. Ewing, J.P. Stone, J.R. Spann, E.W. Steinkuller, D.D. Williams, and R.R. Miller, NRL Report 6233, September 24, 1965.

TABLE I

THIRD STAGE NOZZLE COORDINATES

Pitch Section

X	Y		X	Y
0.	0.		-.75	.7325
-.0075	.025		-.775	.72
-.016	.05		-.8	.7
-.023	.075		-.819	.675
-.031	.1		-.831	.65
-.039	.125		-.837	.625
-.048	.15		-.836	.6
-.056	.175		-.828	.575
-.065	.2		-.814	.55
-.075	.225		-.791	.525
-.084	.25		-.775	.512
-.094	.275		-.75	.497
-.104	.3		-.725	.484
-.115	.325		-.7	.474
-.126	.35		-.675	.467
-.1375	.375		-.65	.461
-.15	.4		-.625	.456
-.162	.425		-.6	.451
-.175	.45		-.575	.446
-.189	.475		-.55	.441
-.203	.5		-.525	.434
-.219	.525		-.5	.4275
-.236	.55		-.475	.42
-.254	.575		-.45	.412
-.276	.6		-.425	.402
-.301	.625		-.4	.39
-.325	.646		-.375	.3775
-.35	.667		-.35	.363
-.375	.685		-.325	.343
-.4	.7		-.3	.332
-.425	.713		-.275	.314
-.45	.725		-.25	.296
-.475	.735		-.225	.277
-.5	.742		-.194	.25
-.525	.7475		-.168	.225
-.55	.751		-.144	.2
-.575	.753		-.123	.175
-.6	.755		-.103	.15
-.625	.755		-.086	.125
-.65	.754		-.069	.1
-.675	.752		-.055	.075
-.7	.7475		-.041	.05
-.725	.742		-.028	.025
			-.013	-.006

TABLE I (Continued)

Section	Radius	d_o	Spacing
N1	4.11	.2119	.5865
N2	4.665	.2461	.6657
N3	5.22	.280	.7453

Coordinates are for N2 Section.

Constant Cross Section, Linear Twist.

All Trailing Edge Radii = .0075 in.

TABLE II

THIRD STAGE ROTOR BLADE COORDINATES

Rotor Tip Section T5

Suction Surface		Pressure Surface	
X	Y	X	Y
-.77	.456	-.755	.430
-.75	.473	-.725	.439
-.725	.493	-.7	.446
-.70	.51	-.675	.451
-.675	.525	-.65	.455
-.65	.5375	-.625	.457
-.625	.5475	-.6	.457
-.6	.556	-.575	.455
-.575	.5625	-.55	.451
-.55	.5675	-.525	.445
-.525	.57	-.5	.4375
-.5	.57	-.475	.428
-.475	.568	-.45	.4175
-.45	.563	-.425	.405
-.425	.556	-.4	.391
-.4	.546	-.375	.375
-.375	.534	-.35	.359
-.35	.52	-.325	.341
-.325	.504	-.3	.3225
-.3	.486	-.275	.3025
-.275	.464	-.25	.281
-.25	.438	-.225	.258
-.225	.409	-.2	.234
-.2	.379	-.175	.208
-.175	.346	-.15	.182
-.15	.308	-.125	.1525
-.125	.269	-.1	.122
-.1	.225	-.075	.089
-.075	.1775	-.05	.055
-.05	.126	-.025	.021
-.025	.071	-.013	.003
-.001	.012		

TABLE II (Continued)

Rotor Pitch - Tip Section T4

Suction Surface		Pressure Surface	
X	Y	X	Y
-.79	.375	-.775	.346
-.775	.389	-.75	.356
-.75	.412	-.725	.364
-.725	.4225	-.7	.372
-.7	.452	-.675	.378
-.675	.468	-.65	.382
-.65	.483	-.625	.385
-.625	.496	-.6	.387
-.6	.507	-.575	.387
-.575	.516	-.55	.385
-.55	.522	-.525	.382
-.525	.526	-.5	.377
-.5	.5275	-.475	.370
-.475	.525	-.45	.3625
-.45	.522	-.425	.353
-.425	.516	-.4	.343
-.4	.509	-.375	.332
-.375	.500	-.35	.320
-.35	.489	-.325	.306
-.325	.476	-.3	.291
-.3	.460	-.275	.275
-.275	.442	-.25	.2575
-.25	.420	-.225	.239
-.225	.3925	-.2	.220
-.2	.363	-.175	.199
-.175	.3325	-.15	.176
-.15	.298	-.125	.150
-.125	.2575	-.1	.1225
-.1	.215	-.075	.092
-.075	.1675	-.05	.0575
-.05	.117	-.025	.021
-.025	.0625	-.013	.003
-.001	.012		

TABLE II (Continued)

Rotor Pitch Section T-3

Suction Surface			Pressure Surface	
X	Y		X	Y
-.825	.2825		-.805	.259
-.8	.311		-.775	.276
-.775	.338		-.75	.288
-.75	.362		-.725	.299
-.725	.385		-.7	.308
-.7	.405		-.675	.316
-.675	.422		-.65	.322
-.65	.437		-.625	.325
-.625	.449		-.6	.328
-.6	.460		-.575	.328
-.575	.467		-.55	.3275
-.55	.473		-.525	.326
-.525	.477		-.5	.323
-.5	.480		-.475	.320
-.475	.481		-.45	.315
-.45	.481		-.425	.309
-.425	.479		-.40	.302
-.4	.474		-.375	.2925
-.375	.466		-.35	.2825
-.35	.457		-.325	.272
-.325	.445		-.3	.260
-.3	.432		-.275	.2475
-.275	.416		-.25	.234
-.25	.398		-.225	.219
-.225	.377		-.2	.203
-.2	.352		-.175	.185
-.175	.3225		-.15	.165
-.15	.289		-.125	.141
-.125	.250		-.1	.114
-.1	.208		-.075	.085
-.075	.1625		-.05	.053
-.05	.113		-.025	.02
-.025	.062		-.013	.003
-.001	.01			

TABLE II (Continued)

Rotor Pitch Root Section T-2

Suction Surface			Pressure Surface	
X	Y		X	Y
-.8925	.0855		-.855	.085
-.8875	.0945		-.85	.0895
-.875	.115		-.825	.110
-.85	.155		-.8	.128
-.825	.1925		-.775	.145
-.8	.225		-.75	.1605
-.775	.255		-.725	.1748
-.75	.2822		-.7	.1875
-.725	.3055		-.675	.1988
-.7	.3265		-.65	.2088
-.675	.3445		-.625	.2175
-.65	.360		-.6	.225
-.625	.3735		-.575	.2308
-.6	.385		-.55	.2358
-.575	.395		-.525	.2398
-.55	.4025		-.5	.242
-.525	.4088		-.475	.243
-.5	.413		-.45	.2432
-.45	.416		-.4	.2405
-.4	.412		-.35	.2325
-.35	.3995		-.3	.2205
-.3	.3785		-.25	.2026
-.25	.3485		-.2	.1785
-.2	.3075		-.175	.1632
-.175	.2818		-.15	.1464
-.15	.2522		-.125	.1272
-.125	.2198		-.1	.1055
-.1	.1825		-.075	.0812
-.075	.1442		-.05	.0528
-.05	.1025		-.025	.0195
-.025	.0575		-.017	.0075
0	.009			
.0045	.005			
.01	0			

TABLE II (Continued)

Rotor Root Section T-1

Suction Surface		Pressure Surface	
X	Y	X	Y
-.8925	.0855	-.855	.085
-.8875	.0945	-.85	.0895
-.875	.115	-.825	.110
-.85	.155	-.8	.128
-.825	.1925	-.775	.145
-.8	.225	-.75	.1605
-.775	.255	-.725	.1748
-.75	.2822	-.7	.1875
-.725	.3055	-.675	.1988
-.7	.3265	-.65	.2088
-.675	.3445	-.625	.2175
-.65	.360	-.6	.225
-.625	.3735	-.575	.2308
-.6	.385	-.55	.2358
-.575	.395	-.525	.2398
-.55	.4025	-.5	.242
-.525	.4088	-.475	.243
-.5	.413	-.45	.2432
-.45	.416	-.4	.2405
-.4	.412	-.35	.2325
-.35	.3995	-.3	.2205
-.3	.3785	-.25	.2026
-.25	.3485	-.2	.1785
-.2	.3075	-.175	.1632
-.175	.2818	-.15	.1464
-.15	.2522	-.125	.1272
-.125	.2198	-.1	.1055
-.1	.1825	-.075	.0812
-.075	.1442	-.05	.0528
-.05	.1025	-.025	.0195
-.025	.0575	-.017	.0075
0	.009		
.0045	.005		
.01	0		

TABLE II (Continued)

Section	Radius	Spacing	Angle of Leading Edge Ellipse	d_o	Stacking Point
T5	5.15	.6223	28.96	.3021	X = -.368
					Y = .397
T4	4.89	.5909	36.50	.2915	X = -.390
					Y = .363
T3	4.63	.5594	42.20	.2801	X = -.413
					Y = .332
T2	4.37	.5280	47.20	.2704	X = -.436
					Y = .299
T1	4.11	.4966	51.80	.2678	X = -.457
					Y = .269

All trailing edge radii - .0075.

All leading edges formed by 0.070 x 0.035 ellipse.

TABLE III.

THREE-STAGE POTASSIUM TURBINE TESTING - 3000 KW FACILITY

Item No.	Parameter	Loca-tion	Sta-tion	Range	Sensor	Control Room Readout	Digital Readout Channel	Channel or Position
1	Vapor Temperature	045°	1	1400-1650°F	CA T/C	Digital		
2	Vapor Temperature	135°	1	1400-1650°F	CA T/C	Digital		
3	Vapor Temperature	235°	1	1400-1650°F	CA T/C	Digital		
4	Vapor Temperature	315°	1	1400-1650°F	CA T/C	Digital		
5	Vapor Static Pressure	0°	1	0-50 psia				
6	Vapor Static Pressure	0°	1	0-50 psia	Efflux	Digital		
7	Vapor Static Pressure	0°	1	0-50 psia	Efflux	Digital		
8	Vapor Static Pressure	270°	1	0-50 psia	Taylor & Pace	Digital		
9	Vapor Total Pressure	080°	1	0-50 psia	Efflux	Digital		
10	Vapor Total Pressure	280°	1	0-50 psia	Efflux	Digital		
11	Vapor Temperature	55°	3	1400-1650°F	CA T/C	Digital		
12	Vapor Temperature	145°	3	1400-1650°F	CA T/C	Digital		
13	Vapor Temperature	235°	3	1400-1650°F	CA T/C	Digital		
14	Vapor Temperature	325°	3	1400-1650°F	CA T/C	Digital		
15	Vapor Static Pressure	80°	3	0-50 psia	Efflux	Digital		
16	Vapor Static Pressure	170°	3	0-50 psia	Efflux	Digital		
17	Vapor Static Pressure	260°	3	0-50 psia	Efflux	Digital		
18	Vapor Static Pressure	350°	3	0-50 psia	Efflux	Digital		
19	Vapor Total Pressure	0°	3	0-50 psia	Efflux	Digital		
20	Vapor Total Pressure	90°	3	0-50 psia	Efflux	Digital		
21	Vapor Total Pressure	180°	3	0-50 psia	Efflux	Digital		
22	Vapor Total Pressure	270°	3	0-50 psia	Efflux	Digital		
23	Vapor Temperature	127°	4	1300-1650°F	CA T/C	Digital		
24	Vapor Temperature	314°	4	1300-1650°F	CA T/C	Digital		
25	Vapor Static Pressure	83° Inner	4	0-50 psia	Efflux	Digital		

Item No.	Parameter	Loca-tion	Sta-tion	Range	Sensor	Control Room Readout	Digital Readout Channel	Channel or Position
26	Vapor Static Pressure	18° Outer	4	0-50 psia	Efflux	Digital		
27	Vapor Static Pressure	85° Outer	4	0-50 psia	Efflux	Digital		
28	Vapor Static Pressure	280° Outer	4	0-50 psia	Efflux	Digital		
29	Vapor Static Pressure	281° Inner	4	0-50 psia	Efflux	Digital		
30	Vapor Temperature	138°	5	650-1650°F	CA T/C	Digital		
31	Vapor Temperature	315°	5	650-1650°F	CA T/C	Digital		
32	Vapor Static Pressure	82° Inner	5	0-50 psia	Efflux	Digital		
33	Vapor Static Pressure	277° Outer	5	0-50 psia	Efflux	Digital		
34	Vapor Static Pressure	278° Inner	5	0-50 psia	Efflux	Digital		
35	Vapor Temperature	48°	6	650-1650°F	CA T/C	Digital		
36	Vapor Temperature	215°	6	650-1650°F	CA T/C	Digital		
37	Vapor Static Pressure	79° Outer	6	0-50 psia	Efflux	Digital		
38	Vapor Static Pressure	28° Outer	6	0-50 psia	Efflux	Digital		
39	Vapor Static Pressure	82° Inner	6	0-50 psia	Efflux	Digital		
40	Vapor Static Pressure	280° Outer	6	0-50 psia	Efflux	Digital		
41	Vapor Static Pressure	277° Inner	6	0-50 psia	Efflux	Digital		
42	Vapor Temperature	303°	7	650-1650°F	CA T/C	Digital		
43	Vapor Temperature	142°	7	650-1650°F	CA T/C	Digital		
44	Vapor Static Pressure	278° Outer	7	0-50 psia	Efflux	Digital		
45	Vapor Static Pressure	82° Inner	7	0-50 psia	Efflux	Digital		
46	Vapor Static Pressure	279° Inner	7	0-50 psia	Efflux	Digital		
47	Vapor Temperature	48°	8	650-1650°F	CA T/C	Digital		
48	Vapor Temperature	230°	8	650-1650°F	CA T/C	Digital		
49	Vapor Static Pressure	20° Outer	8	0-50 psia	Efflux	Digital		
50	Vapor Static Pressure	83° Outer	8	0-50 psia	Efflux	Digital		

Item No.	Parameter	Location	Station	Range	Sensor	Control Room Readout	Digital Readout Channel	Channel or Position
51	Vapor Static Pressure	276° Outer	8	0-50 psia	Efflux	Digital		
52	Vapor Static Pressure	78° Inner	8	0-50 psia	Efflux	Digital		
53	Vapor Static Pressure	274° Inner	8	0-50 psia	Efflux	Digital		
54	Vapor Temperature	105°	9	650-1650°F	CA T/C	Digital		
55	Vapor Temperature	255°	9	650-1650°F	CA T/C	Digital		
56	Vapor Static Pressure	55°	9	0-50 psia	Efflux	Digital		
57	Vapor Static Pressure	65°	9	0-50 psia	Efflux	Digital		
58	Vapor Static Pressure	295°	9	0-50 psia	Efflux	Digital		
59	Vapor Static Pressure	305°	9	0-50 psia	Efflux	Digital		
60	Vapor Total Pressure	8°	9	0-50 psia	Efflux	Digital		
61	Vapor Total Pressure	75°	9	0-50 psia	Efflux	Digital		
62	Vapor Total Pressure	285°	9	0-50 psia	Efflux	Digital		
63	Vapor Total Pressure	352°	9	0-50 psia	Efflux	Digital		
64	Vapor Temperature	120°	9.5	650-1650°F	CA T/C	Digital		
65	Vapor Temperature	240°	9.5	650-1650°F	CA T/C	Digital		
66	Vapor Static Pressure	25° Inner	9.5	0-50 psia	Efflux	Digital		
67	Vapor Static Pressure	45° Outer	9.5	0-50 psia	Efflux	Digital		
68	Vapor Static Pressure	315° Outer	9.5	0-50 psia	Efflux	Digital		
69	Vapor Static Pressure	335° Inner	9.5	0-50 psia	Efflux	Digital		
70	Vapor Total Pressure	15°	9.5	0-50 psia	Efflux	Digital		
71	Vapor Total Pressure	345°	9.5	0-50 psia	Efflux	Digital		
72	Vapor Temperature	82°	9.6	650-1650°F	CA T/C	Digital		
73	Vapor Temperature	278°	9.6	650-1650°F	CA T/C	Digital		
74	Vapor Static Pressure	0°	9.6	0-50 psia				
75	Vapor Static Pressure	60°	9.6	0-50 psia	Efflux	Digital		

Item No.	Parameter	Location	Station	Range	Sensor	Control Room Readout	Digital Readout Channel	Channel or Position
76	Vapor Static Pressure	125°	9.6	0-50 psia	Efflux	Digital		
77	Vapor Static Pressure	235°	9.6	0-50 psia	Efflux	Digital		
78	Vapor Static Pressure	300°	9.6	0-50 psia	Efflux	Digital		
79	Vapor Temperature	SW	10	650-1650°F	CA T/C	Digital		
80	Vapor Temperature	SE	10	650-1650°F	CA T/C	Digital		
81	Vapor Temperature	NE	10	650-1650°F	CA T/C	Digital		
82	Vapor Temperature	NW	10	650-1650°F	CA T/C	Digital		
83	Vapor Static Pressure	SE	10	0-20 psia				
84	Vapor Static Pressure	NE	10	0-20 psia	Efflux	Digital		
85	Vapor Static Pressure	N	10	0-20 psia	Taylor	Digital		
86	Vapor Total Pressure	W	10	0-20 psia	Efflux	Digital		
87	Vapor Total Pressure	E	10	0-20 psia	Efflux	Digital		
88	Calorimeter Temp.	10°	1	1400-1650°F	CA T/C	Digital		
89	Calorimeter Pres.	10°	1	0-50 psia	Efflux	Digital		
90	Main Condenser Flow	Main EmFm	11	0-10 MV	EmFm	Digital		
91	Main Cond. Flow Temp.	Main EmFm	11	900°F	CA T/C	Digital		
92	Water Brake Torque	Water Brake	11	0-1250 lbs	Bytrex	Dial & Digital		
93	Steam Turb. Torque							
94	Speed	Steam Turb.		0-25,000 rpm	Magn. Pickup	Berkeley		
95	Speed	Pot. Turb.		0-25,000 rpm	Magn. Pickup	Sanborn & Digital		
96	Steam Turbine Inlet Pressure	Steam Turb.		0-100 psig	Pace	Digital		
97	R.T.D. CATS Block Temperature	CATS Block			R.T.D.	Digital		
98	Stand. Resistor R.T.D. Network			5.6 MV		Digital		
99	Pad Bearing 1 Temperature	Pad Brg 1		250°F	CA T/C	TR#3-1		
100	Pad Bearing 2 Temperature	Pad Brg 2		250°F	CA T/C	TR#3-2		

Item No.	Parameter	Location	Station	Range	Sensor	Control Room Readout	Digital Readout Channel	Channel or Position
101	Pad Bearing 3 Temperature	Pad Brg 3		250°F	CA T/C	TR#3-3		
102	Pad Bearing 4 Temperature	Pad Brg 4		250°F	CA T/C	Sanborn		
103	Pad Bearing 5 Temperature	Pad Brg 5		250°F	CA T/C	TR#3-4		
104	Pad Bearing Ring Temperature	24°		250°F	CA T/C	TR#3-19		
105	Pad Bearing Ring Temperature	50°		250°F	CA T/C	TR#3-20		
106	Pad Bearing Lube Flow	Pad Brg		0-200 H₂0 (36pm)	Foxboro D/P Cell	Sanborn		
107	Pad Bearing Lube Inlet Pressure	Pad Brg			Gauge	Visual & Wrng.Sig.		
108	Pot. Turb. Bearing Lube Temp. Out			250°F	CA T/C	Digital & TR#3-5		
109	Pot. Turb. Bearing Lube Temp. In			250°F	CA T/C	Digital & TR#3-6		
110	Rear Ball Thrust Bearing Temp.	Ball Brg		32°-282°F	CA T/C	Sanborn		
111	Rear Ball Thrust Bearing Temp.	Ball Brg			CA T/C	Spare		
112	Fwd. Ball Thrust Bearing Temp.	Ball Brg		32°-282°F	CA T/C	Sanborn		
113	Fwd. Ball Thrust Bearing Temp.	Ball Brg			CA T/C	TR#3-8		
114	Ball Brg Lube Oil Pressure In			200 psig	Bourdon Gauge	Visual & Wrng.Sig.		
115	Ball Brg. Lube Oil Flow			0-200 H₂0 (36pm)	Foxboro D/P Cell	Sanborn		
116	Turbine Bearing Housing Temp. Fwd.	Brg Hsg			CA T/C	TR#1-4		
117	Turbine Bearing Housing Temp. Mid	Brg Hsg			CA T/C			
118	Turbine Bearing Housing Temp. Aft	Brg Hsg			CA T/C	TR#1-13		
119	Brg. Housing Fwd.	Bot. Cntln.			Skin CA T/C	TR#3-7		
120	Brg. Housing Mid	Bot. Cntln.			Skin CA T/C	TR#3-14		
121	Brg. Housing Aft	Bot. Cntln.			Skin CA T/C	TR#3-15		
122	Acceleration Aft Ring Vert.	Ret Rg 0°		0-10 g's	Accel.	Sanborn		
123	Acceleration Aft Ring Horz.	Ret Rg 270°		0-10 g's	Accel.	Sanborn		
124	Turbine Shaft Radial Movement	Ret Rg 70°			Bentley	Scope		
125	Turbine Shaft Radial Movement	Ret Rg 160°			Bentley	Scope		

Item No.	Parameter	Location	Station	Range	Sensor	Control Room Readout	Digital Readout Channel	Channel or Position
126	Displacement Steam Turb. Aft Brg. Vert			0-5 mils	Vib. Pickup	Sanborn		
127	Displacement Steam Turb. Aft Brg. Horz			0-5 mils	Vib. Pickup	Sanborn		
128	Displacement Pot. Turb. Vertical			0-5 mils	Vib. Pickup	Sanborn		
129	Displacement Pot. Turb. Horz			0-5 mils	Vib. Pickup	Sanborn		
130	Displacement Wtr. Brk. Forward Vert.			0-5 mils	Vib. Pickup	Sanborn		
131	Displacement Wtr. Brk. Forward Horz.			0-5 mils	Vib. Pickup	Sanborn		
132	Steam Turbine Bearing Fwd. Temp.			250°F	CA T/C	TR#3-9		
133	Steam Turbine Bearing Mid. Temp.			250°F	CA T/C	TR#3-10		
134	Steam Turbine Bearing Aft Temperature			250°F	CA T/C	TR#3-11		
135	Steam Turbine Lube In Temperature			250°F	CA T/C	TR#3-12		
136	Steam Turbine Lube Out Temperature			250°F	CA T/C	TR#3-13		
137	Steam Turbine Lube Oil Pressure			80 psig	Bourdon Gauge	Dial & Wrng. Lt.		
138	Steam Turb. & Wtr. Brk. Lube Flow			1 gpm	Flw-Rater	Warning Light		
139	Wtr. Brk. Water Inlet Temperature	Wtr. in-ln		60°F	CA T/C	Digital		
140	Wtr. Brk. Water Inlet Temperature	Wtr. in-ln		60°F	CA T/C	TR#3-14		
141	Wtr. Brk. Water Inlet Temperature	Wtr. in-ln		60°F	CA T/C	Alarm		
142	Wtr. Brk. Water Outlet Temp.	Wtr. in-ln		190°F	CA T/C	Digital		
143	Wtr. Brk. Water Outlet Temp.	Wtr. in-ln		190°F	CA T/C	TR#3-15		
144	Wtr. Brk. Bearing Fwd. Temp.	Wtr. Brk.		180°F	CA T/C	TR#3-16		
145	Water Brake Bearing Aft Temp.	Wtr. Brk.		180°F	CA T/C	TR#3-17		
146	Water Brake Water Flow	Wtr. in-ln			Potter Fw. Met	Digital		
147	Water Brake Water Flow	Wtr. in-ln			D.C. Gener.	Dial		
148	Potassium Seal In Temperature				CA T/C	Digital		
149	Potassium Seal In Temperature				CA T/C	TR#3-18		
150	Potassium Seal Out Temperature				CA T/C	Digital		

Item No.	Parameter	Location	Station	Range	Sensor	Control Room Readout	Digital Readout Channel	Channel or Position
151	Potassium Seal Out Temperature				CA T/C	TI		
152	Slinger Seal Turbine Inlet Press. P-11			0-150 psig	Taylor Gauge	Dial		
153	Oil Side Seal Sump Pressure P-6			0-30 psig	Taylor Gauge	Dial		
154	Pot. Seal Flow			0-5 MV	Pace & EmFm	F.Rec.& Digital		
155	Temperature Argon Seal In			500°F	CA T/C			
156	Turbine Argon Inlet Pressure P-7	L.Seal atMan.		100 psig	Taylor Gauge	Dial		
157	Pot. Side Seal Pressure P-8			-30 Hg to 100 psig	Taylor & Statham	Sanborn & Dial		
158	Argon Header Pressure P-1			0-60 psig	Taylor	Dial		
159	Argon Extraction Flow	Dnstm of VPL-8		0-10 MV	EmFm	Sanborn		
160	Boiler Drum Pres.	Boiler Inlet			Taylor & Wiancko	Sanborn		
161	Boiler Discharge Temperature (Skin)	Upstm VPL-11		1650°F	Skin CA T/C	Digital		
162	Vapor Static Pres.	0°	9		Taylor & Statham	Sanborn & Digital		
163	Boiler Feed Flow	Boiler Input			EmFm	Sanborn		
164	Boiler Feed Temp.	Blr.Feed EmFm			Skin CA T/C			
165	Turbine Casing Fwd. Temp.	Turb. Casing			Skin CA T/C	TR#2-13		
166	Turbine Casing Aft. Temp.	Turb. Casing			skin CA T/C	TR#2-14		
167	8-Inch Vapor Line Temp.	6' Aft of Sp. Line	2	1450°F	Skin CA T/C			
168	8-Inch Vapor Line Temp.	14' Aft of Spy Line	2	1450°F	Skin CA T/C	TR#1-2		
169	Buller Nose Delta P	Btn item 16-20	3	0-1.5 psid	Efflux & Pace	Digital		
170	Bullet Nose Delta P	Btn item 17-21	3	0-1.5 psid	Efflux & Pace	Digital		
171	Calorimeter Pressure	Calori-meter		0-50 psia	Taylor & Pace	Digital		
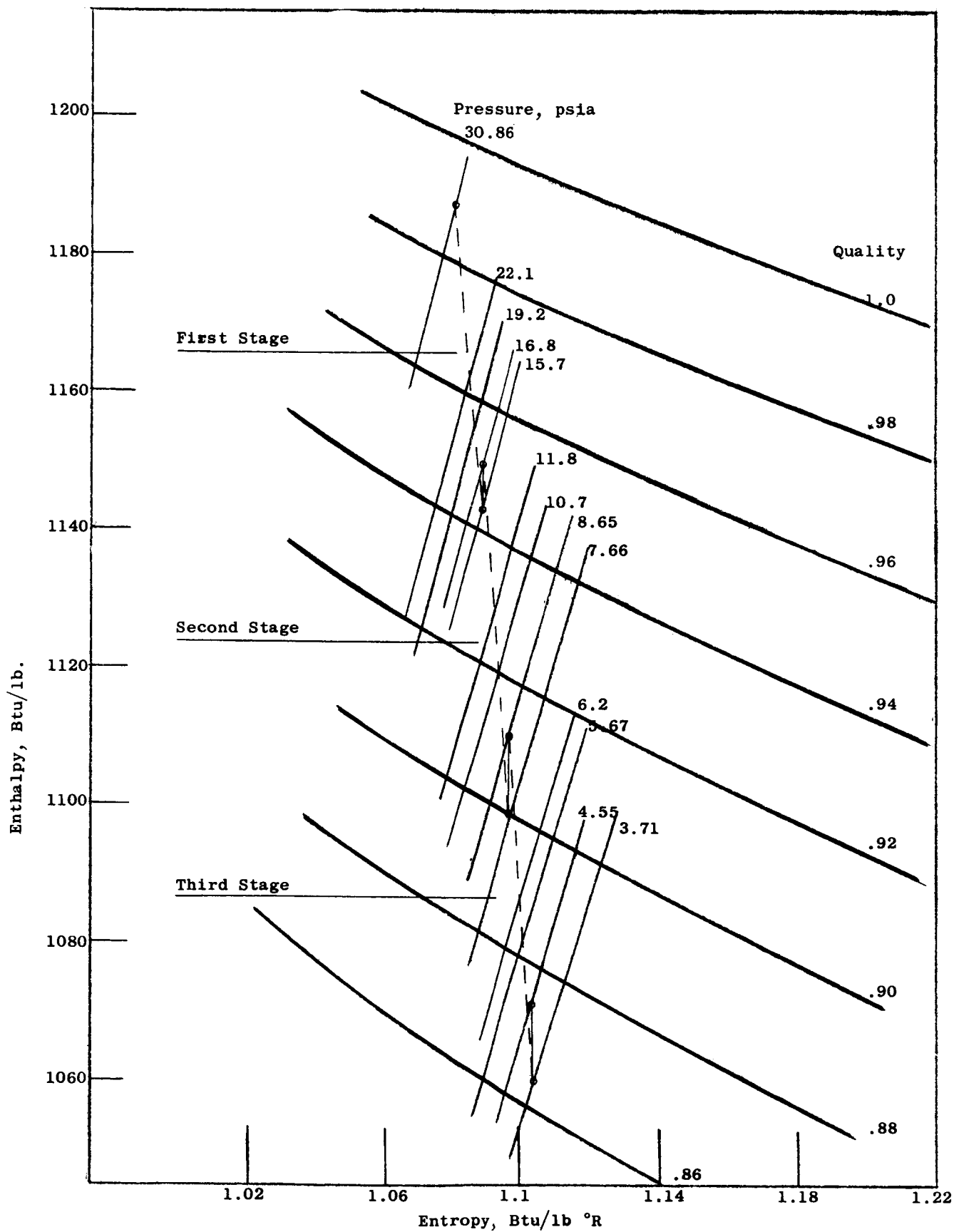
Figure 1. Turbine Expansion on Potassium Mollier Diagram.
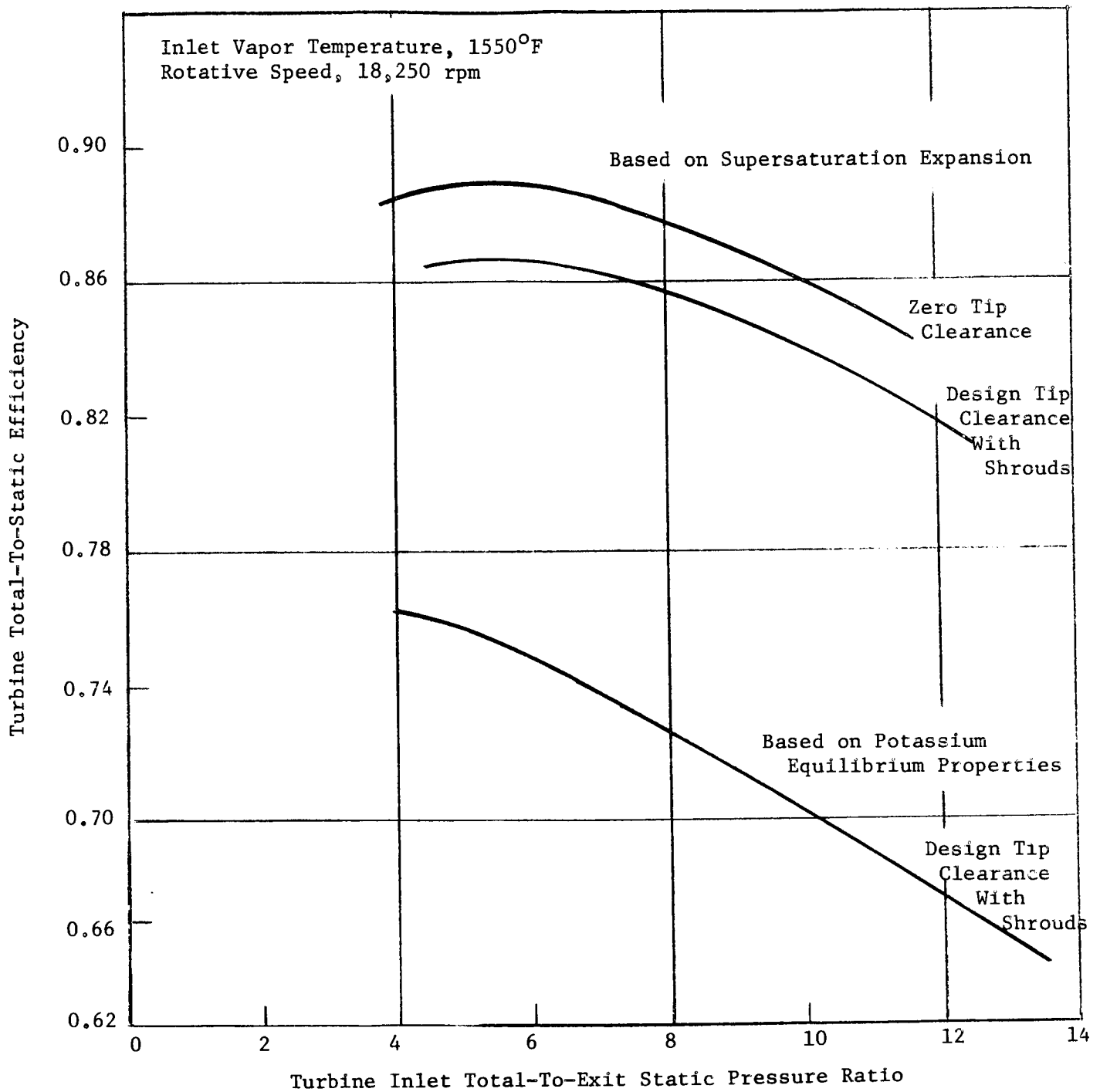
Figure 2. Variation of Turbine Efficiency at Design Conditions.

The figure plots Turbine Total-To-Static Efficiency against Turbine Inlet Total-To-Exit Static Pressure Ratio. Key labels on the chart:

Inlet Vapor Temperature, 1550°F
Rotative Speed, 18,250 rpm

Based on Supersaturation Expansion

Zero Tip Clearance

Design Tip Clearance With Shrouds

Based on Potassium Equilibrium Properties

Design Tip Clearance With Shrouds

8.297
DIA

STG #1 NOZZLE

STG #1 BUCKET

STG #2 NOZZLE

9.680
DIA

9.258
DIA

9.130
DIA

8.920
DIA

8.860
DIA

1.287

.225

.795

.7055

.130

.978

.205

.040

.040

7.316
DIA

7.320
DIA

7.310
DIA

7.410
DIA

7.423
DIA

7.413
DIA

7.423
DIA

7.674
DIA

7.685
DIA

7.675
DIA

7.088
DIA

**Figure 3.   3-Stage Potassium Turbine F
1550°F.**

10.864
DIA

10.932
DIA

10.582
DIA

10.522
DIA

10.076
DIA

9.950

9.740
DIA

STG #3 NOZZLE

STG #3 BUCKET

#2 BUCKET

.913 .137 1.045 .195 .970 1.009 .147

.040

5

7.911
DIA

7.916
DIA

8.028

8.033
DIA

8.020
DIA

7.776
DIA

7.791
DIA

7.906
DIA

7.781
DIA

C 3.00 RAD

UNLESS OTHERWISE SPECIFIED DIMENSIONS ARE IN INCHES— TOLERANCES ON:	SIGNATURES	DAY	MO	YR	GENERAL ELECTRIC
2-PLACE DECIMALS ±		14	2	67	DEPT LOC
3-PLACE DECIMALS ± ALL SURF.					3 STG. POTASSIUM
ANGLES ±					TURBINE HOT FLOWPATH
FRACTIONS ± ✓					
MATERIAL—					

SIZE E CODE IDENT NO. 263E110

SCALE 5X SHEET

Path. Inlet Temperature,
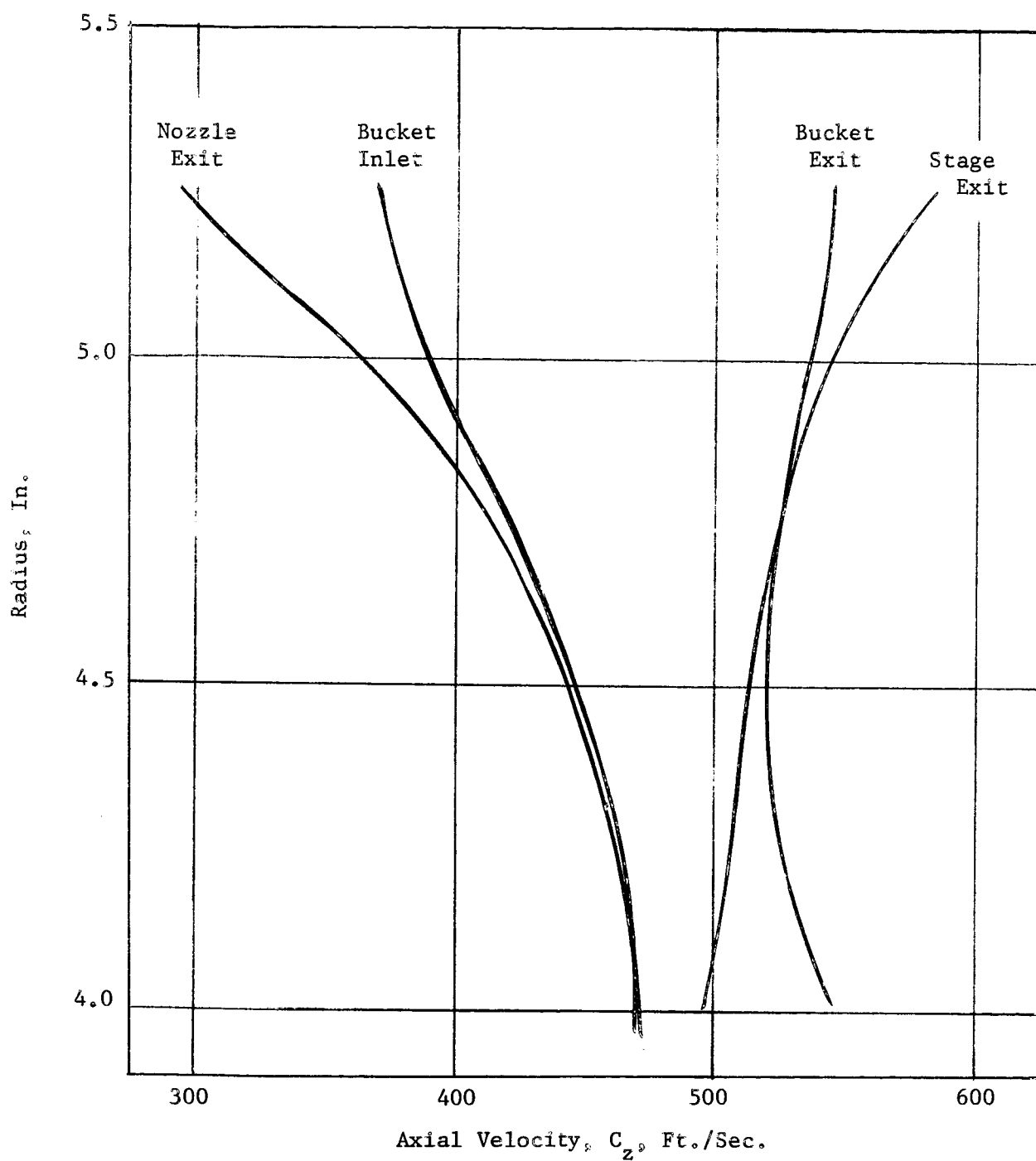
Figure 4. Radial Variation of Axial Velocity in Third Stage.
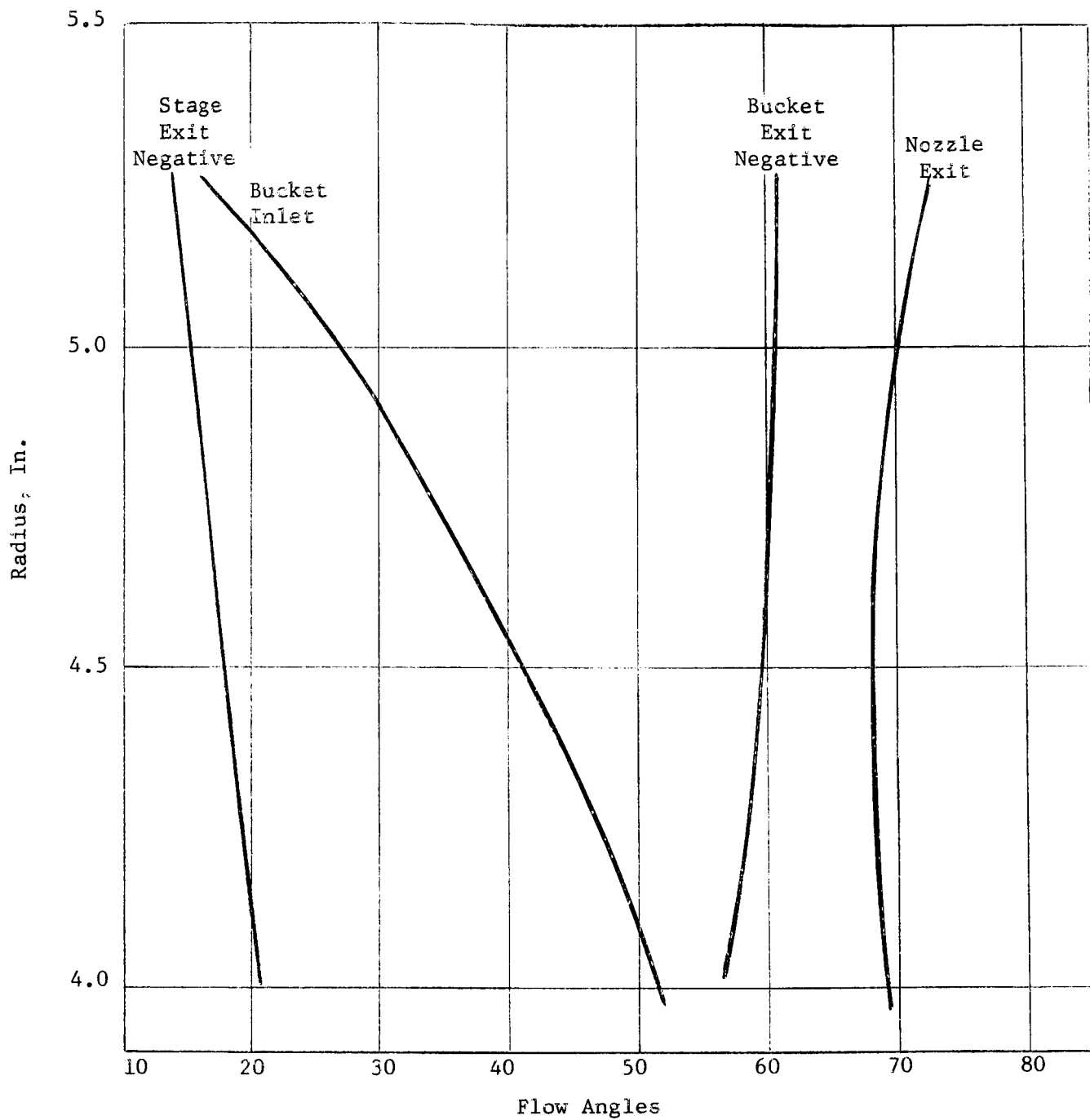
Figure 5. Radial Variation of Flow Angle in Third Stage.
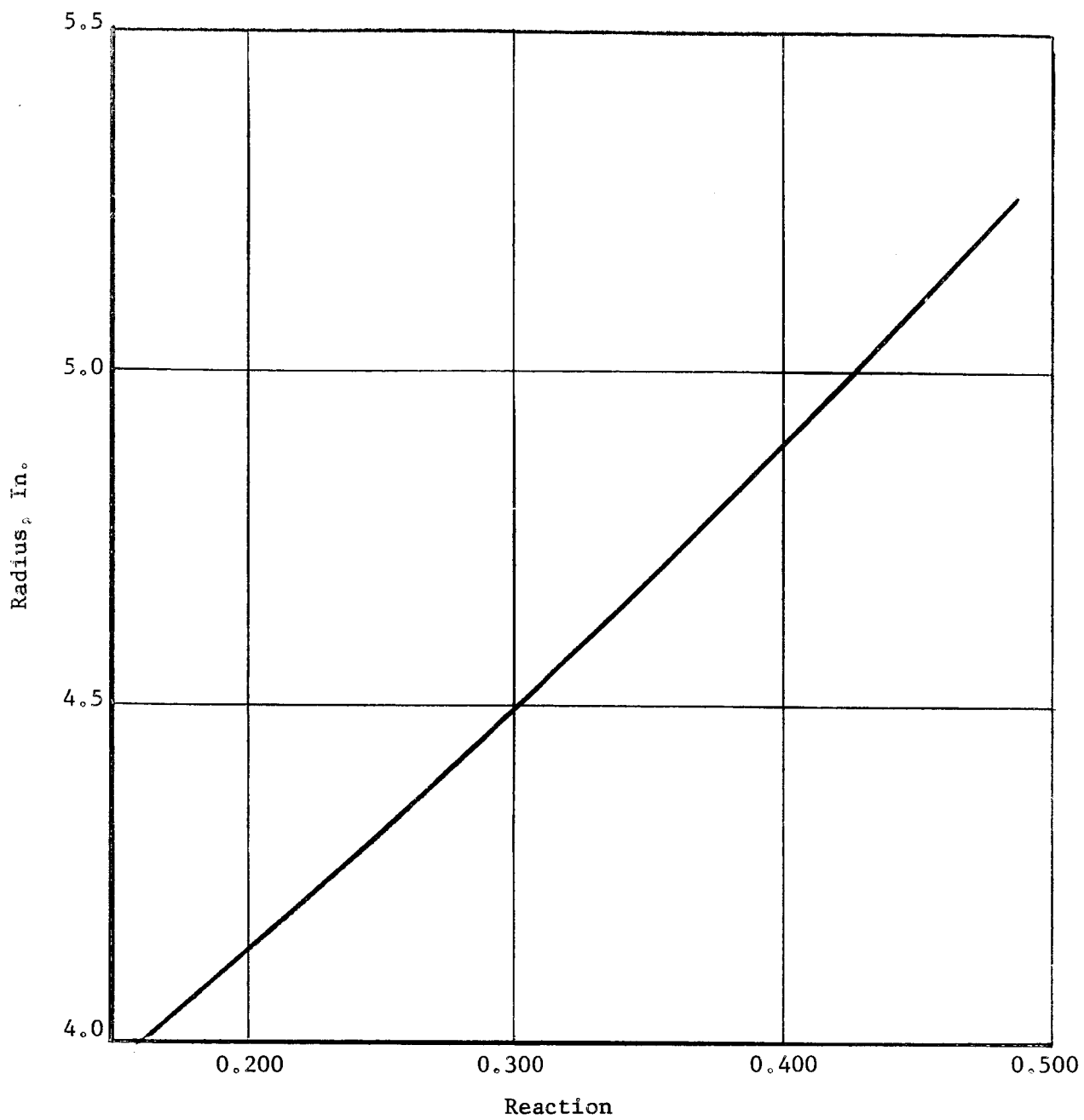
Figure 6. Radial Variation of Stage Reaction in Third Stage.
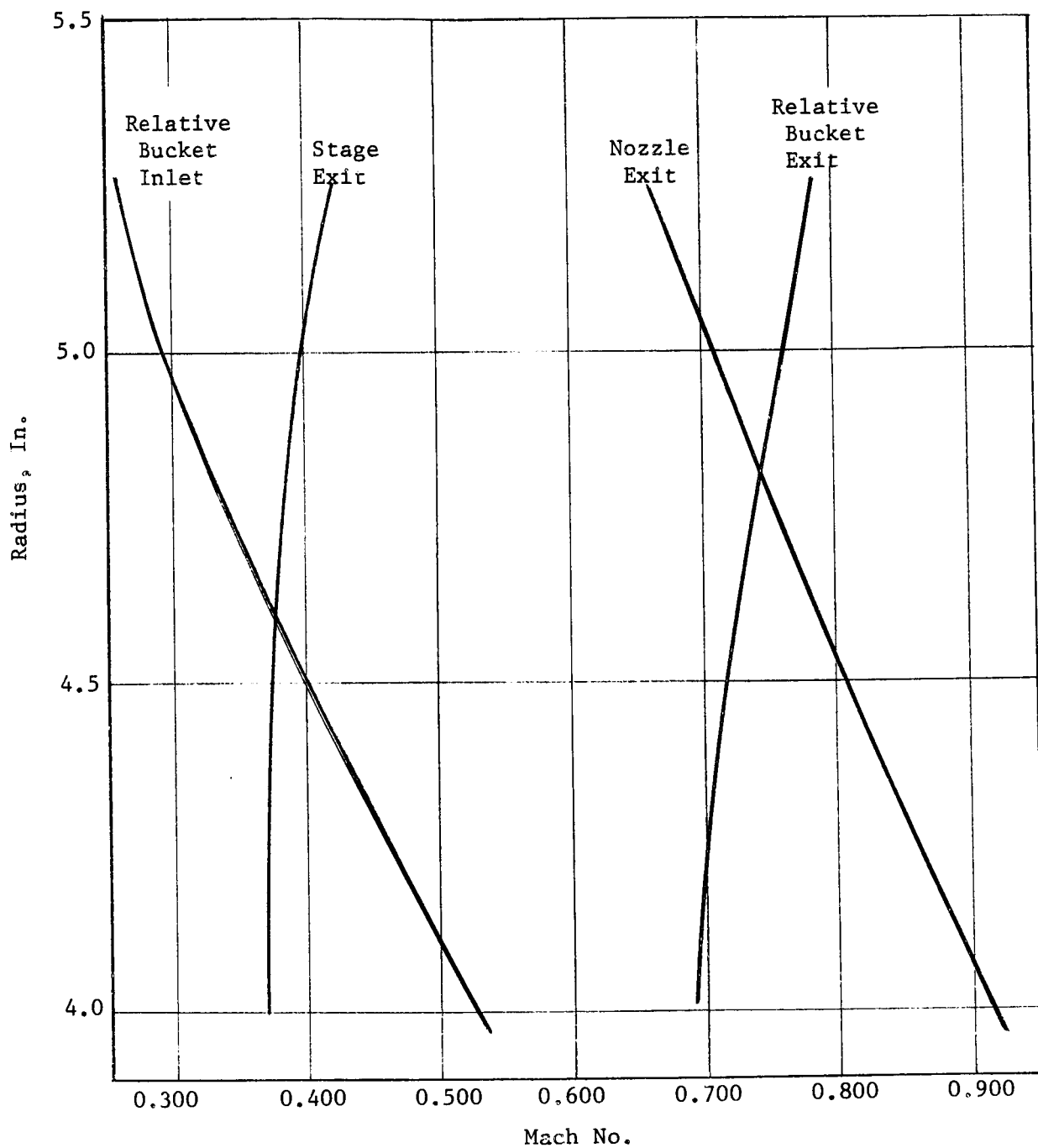
Figure 7. Radial Variation of Mach Number in Third Stage.

Inlet ← → Exit

Absolute
1015
68.5
16
14 6
61
Relative
1121
838
Relative
386 / 371
107 545 563
Absolute
838
Wheel Speed

(a) Tip

1154
68.1
37.5
546
60
1046
17
739
331
431
524 548
160
746

(b) Pitch

1338
52.9
779
69.4
18 9
989
56.5
632
621
470 545 576
186
639
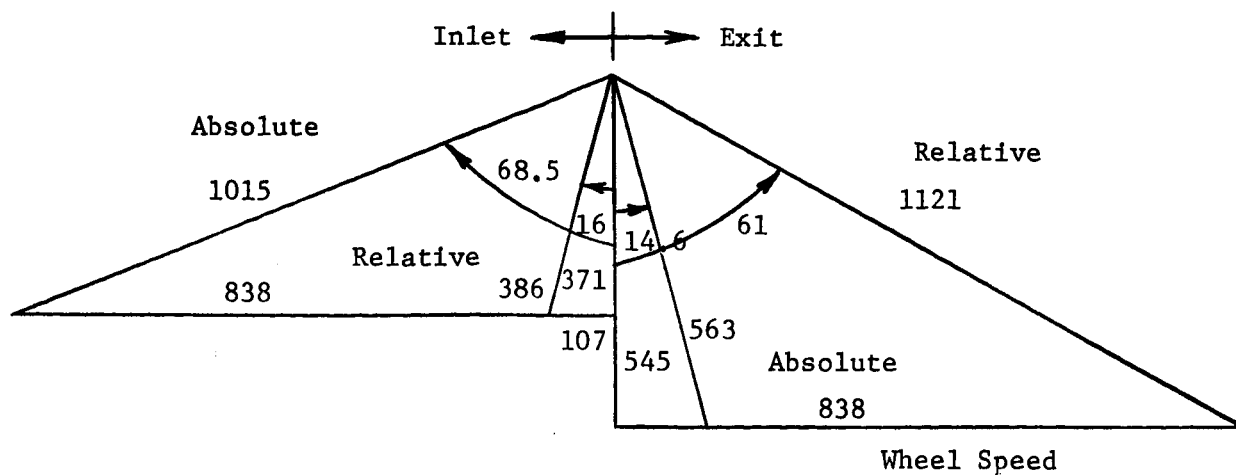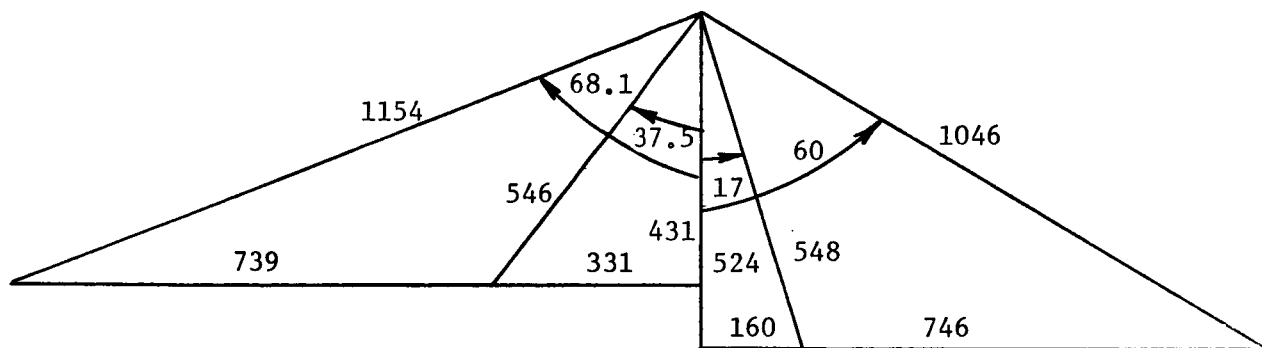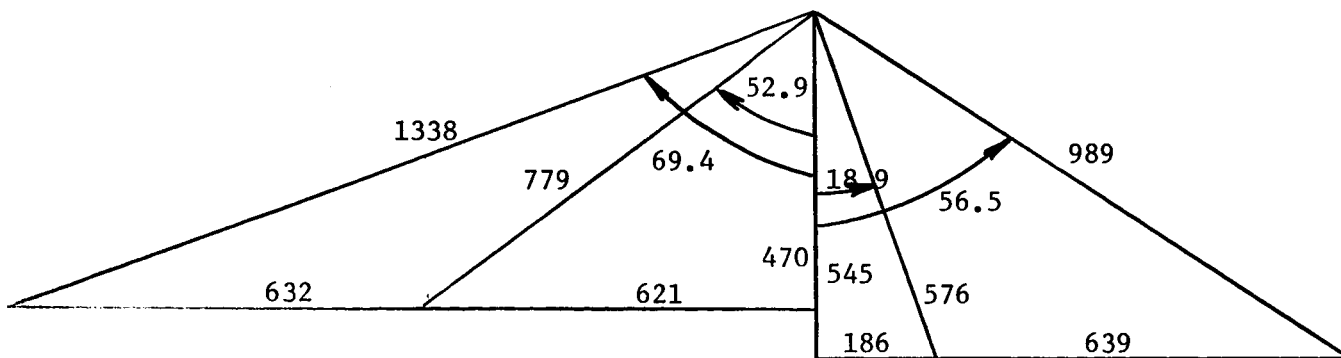
(c) Hub

Figure 8. Third-Stage Design Velocity Diagrams. (Velocities, fps; Angles, Deg.).
Rotative Speed, 18,250 rpm; Inlet Vapor Temperature, 1260°F; Stage
Total Pressure Ratio, 1.845.
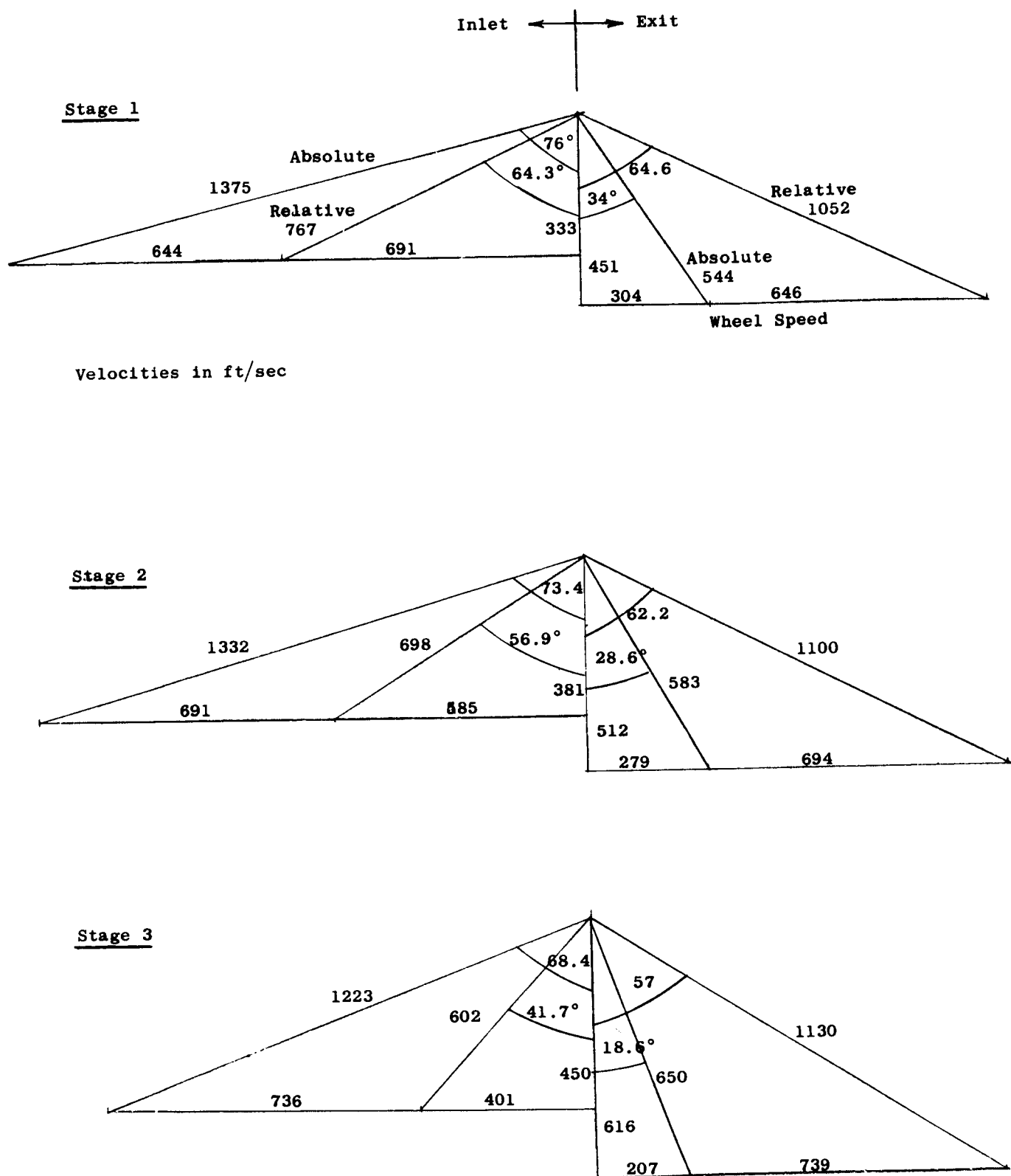
Figure 9. Off Design Mean Line Velocity Diagrams, 18,250 rpm, 1550°F Inlet Temperature, Turbine Inlet Total-to-Exit Static Pressure Ratio, 8.3.
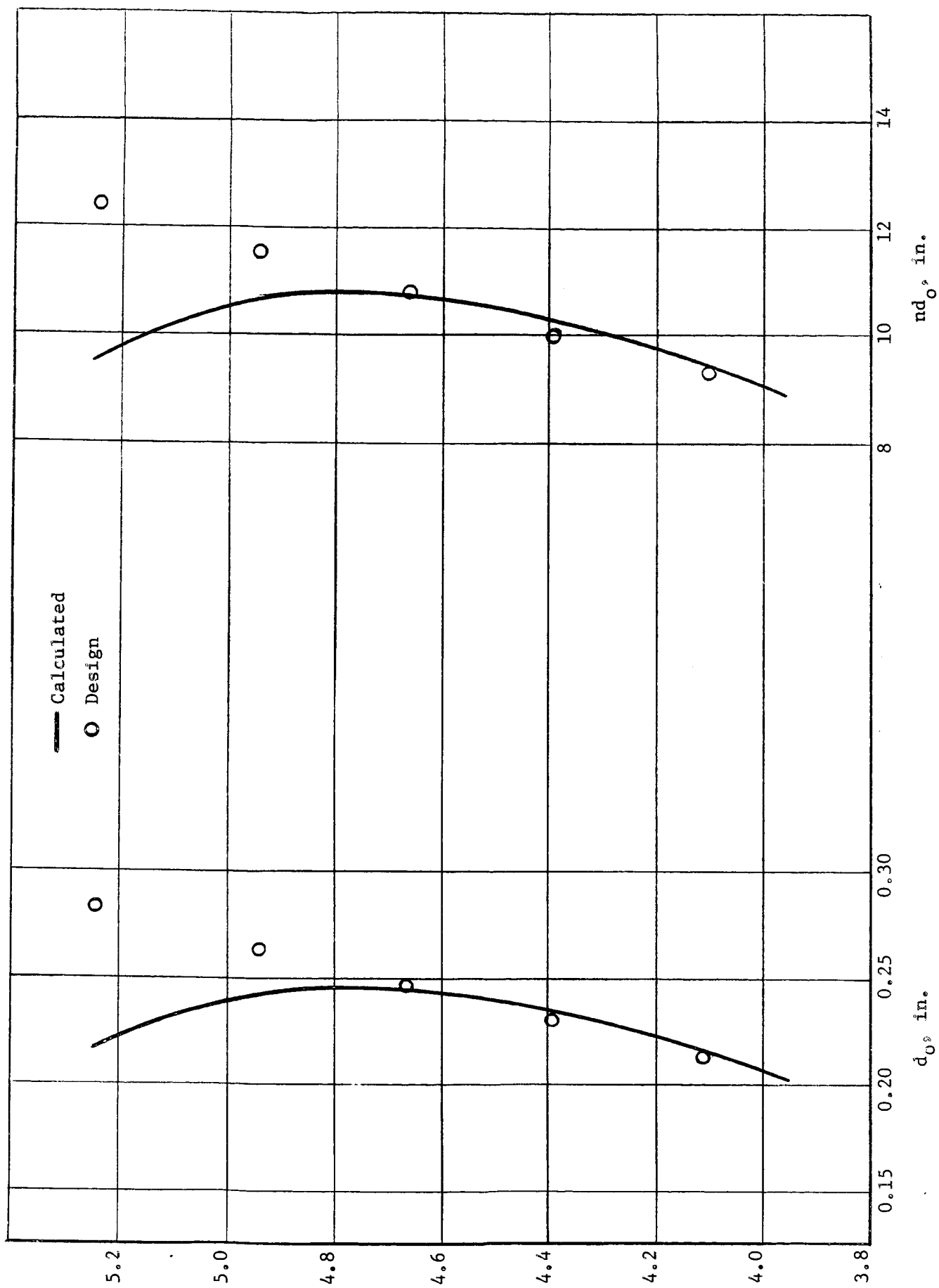
Figure 10. Third Stage Nozzle Throat Dimension.
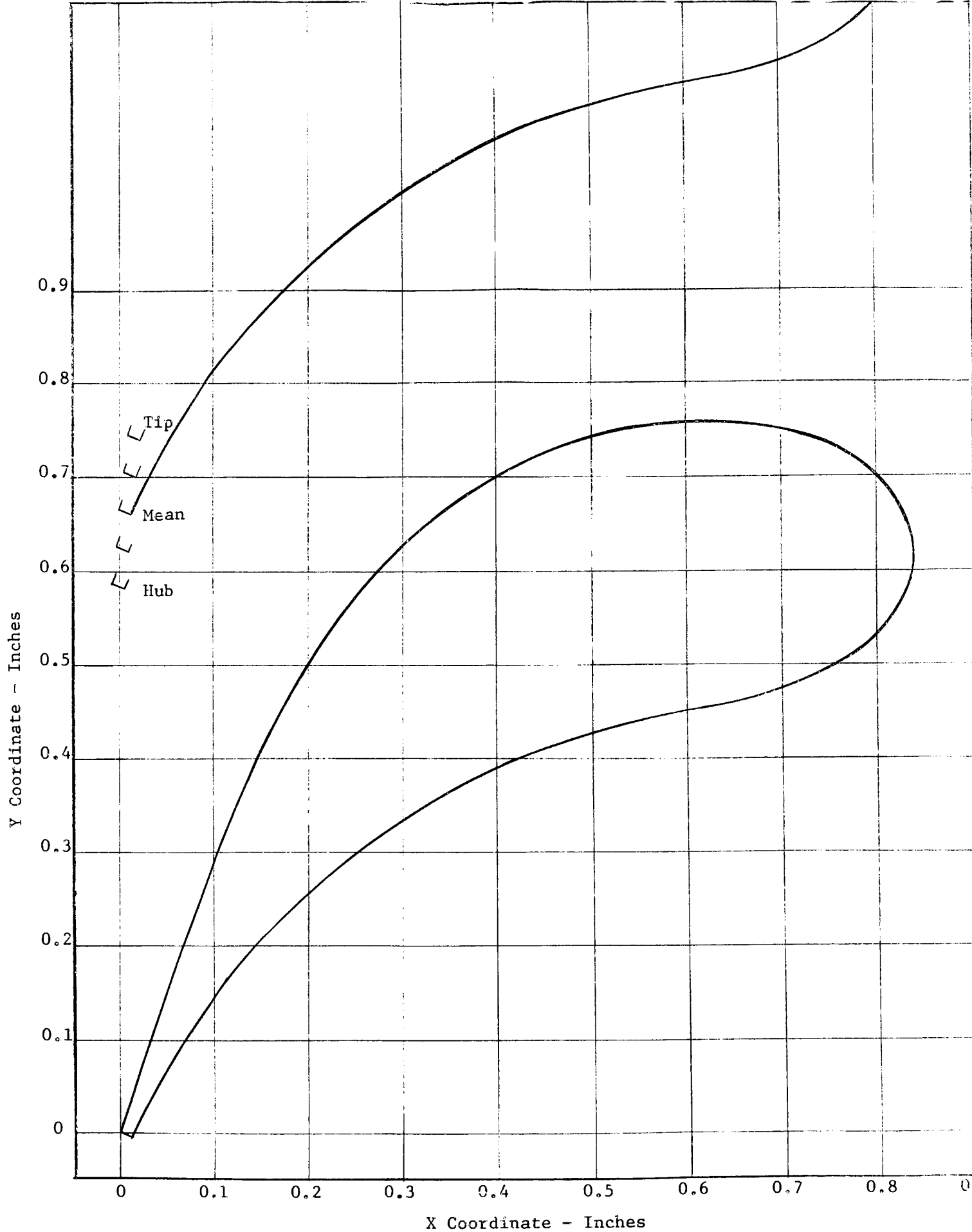
Figure 11. Third Stage Nozzle Mean Section.

Figure 12. Third Stage Nozzle Hub Section Velocity Distribution. -57-
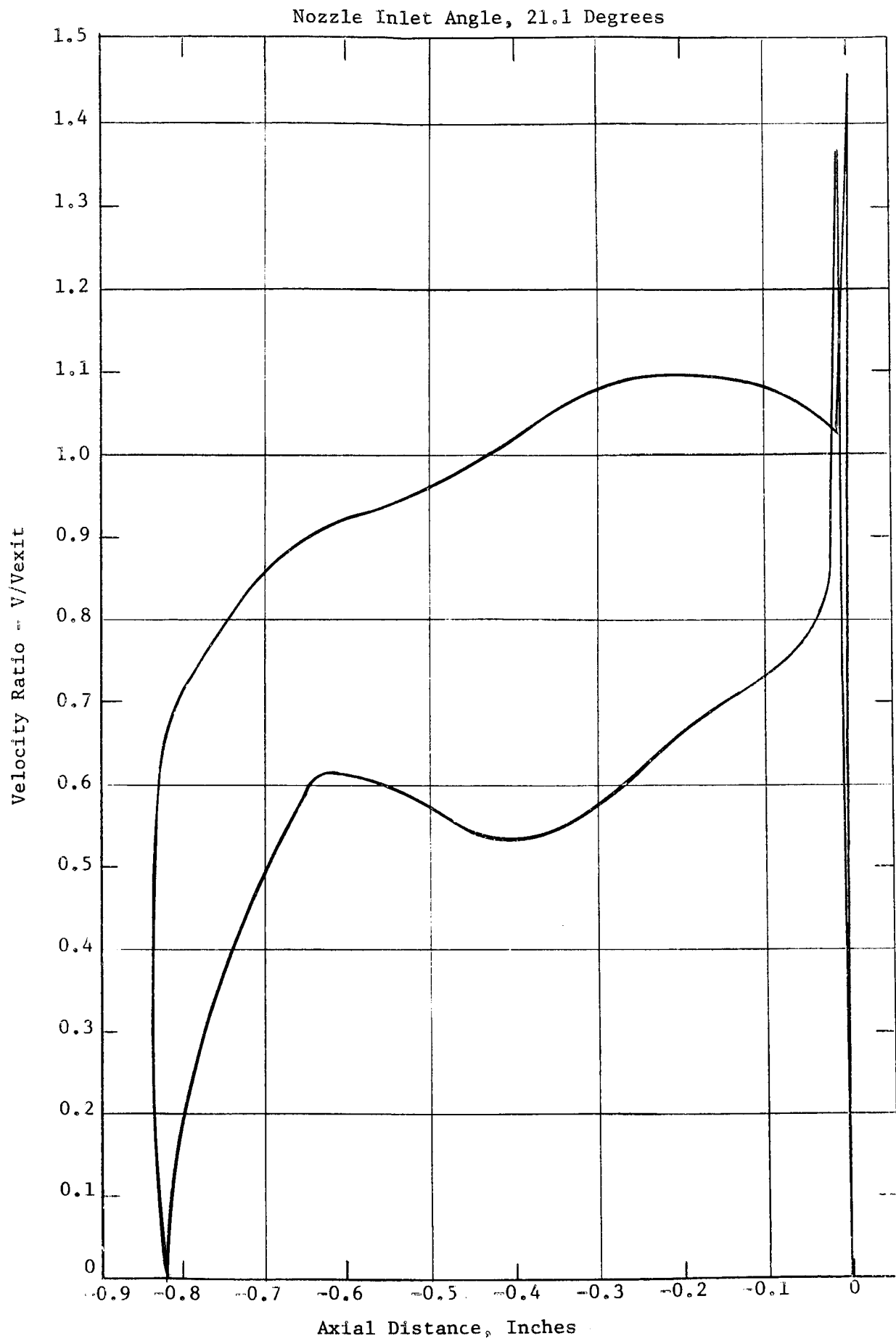
Figure 13. Third Stage Nozzle Mean Section Velocity Distribution.
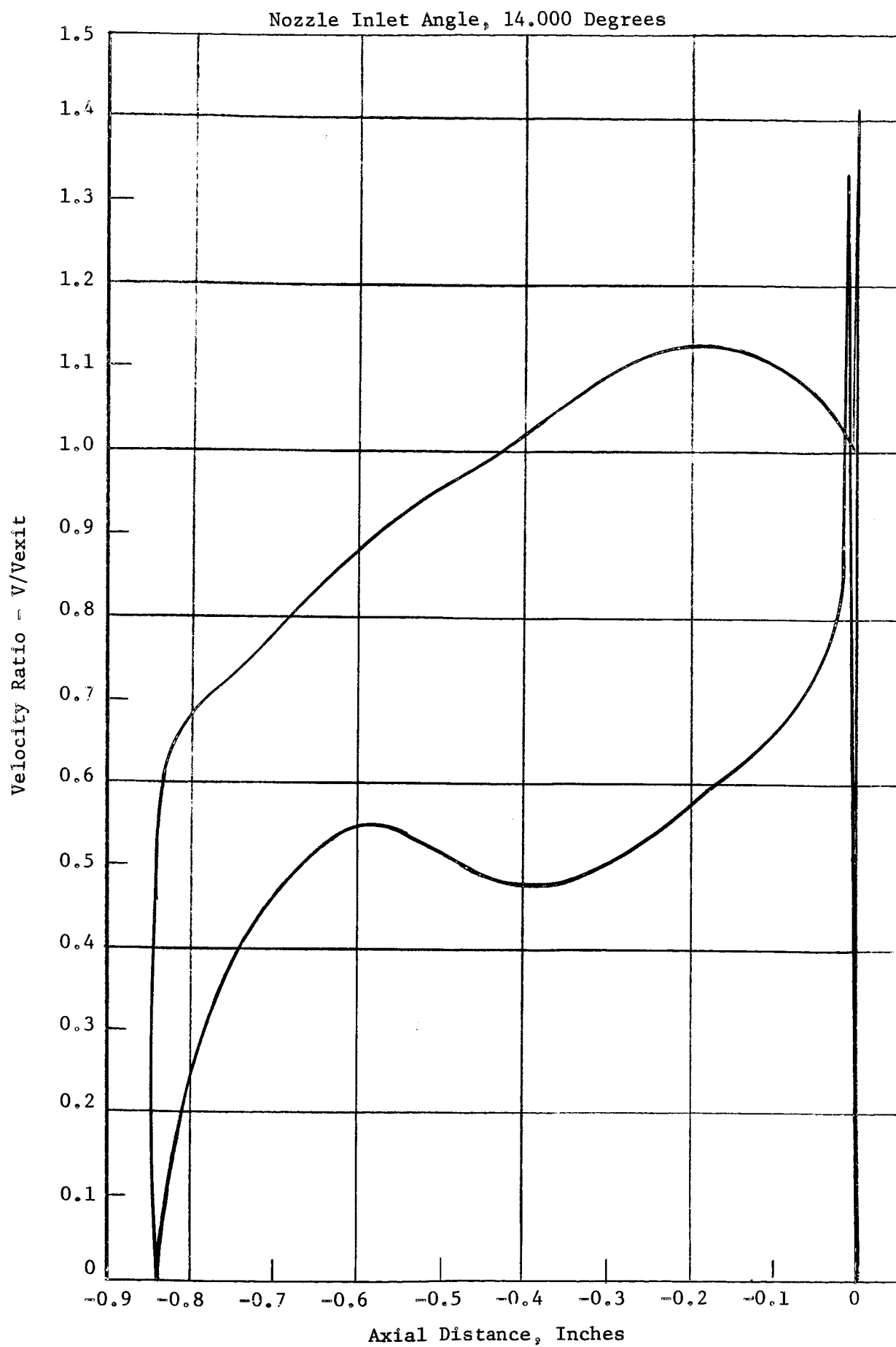
Figure 14. Third Stage Nozzle Tip Section Velocity Distribution.
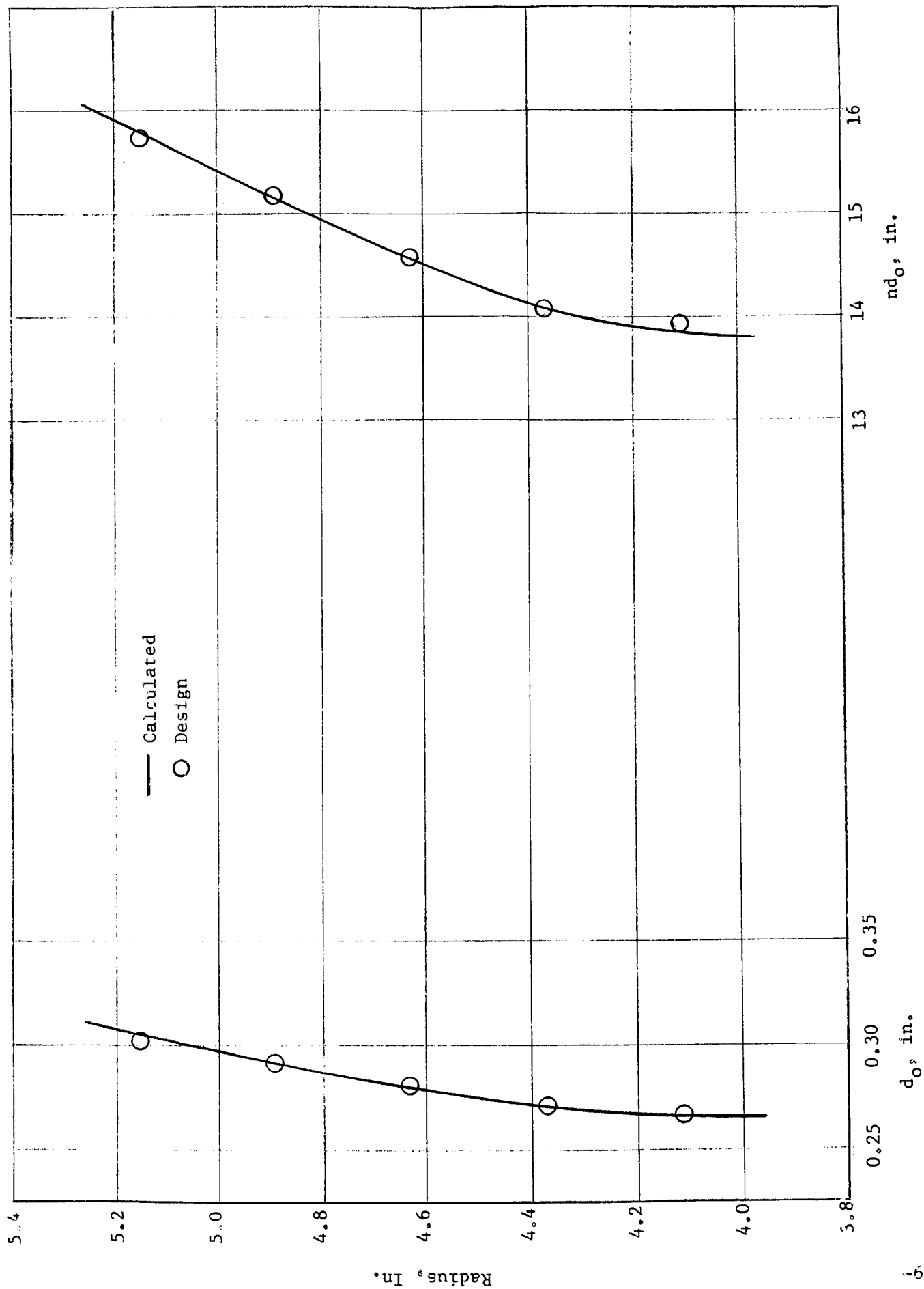
Figure 15. Third Stage Rotor Throat Dimension.
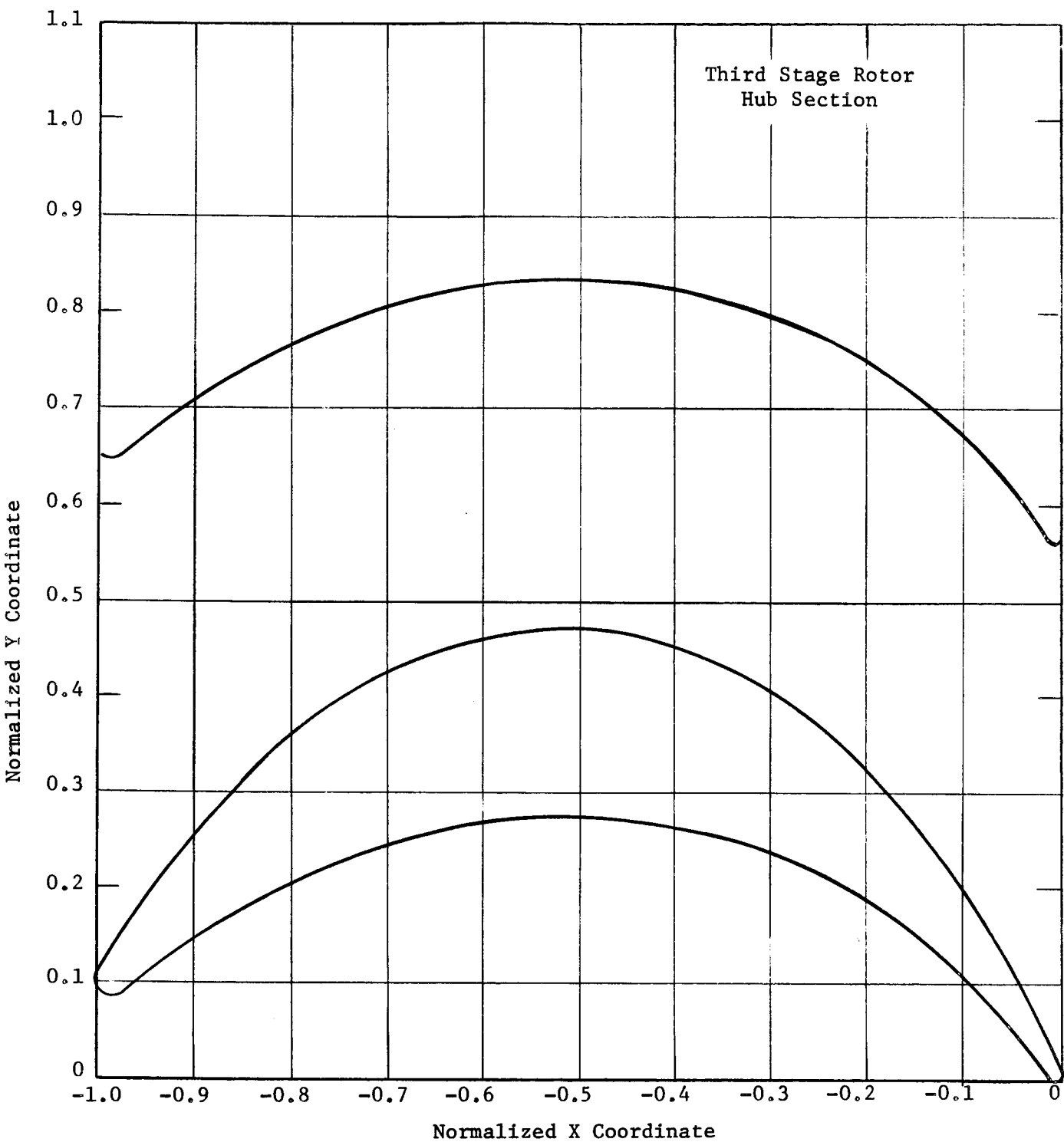
Figure 16. Third Stage Rotor Hub Section.
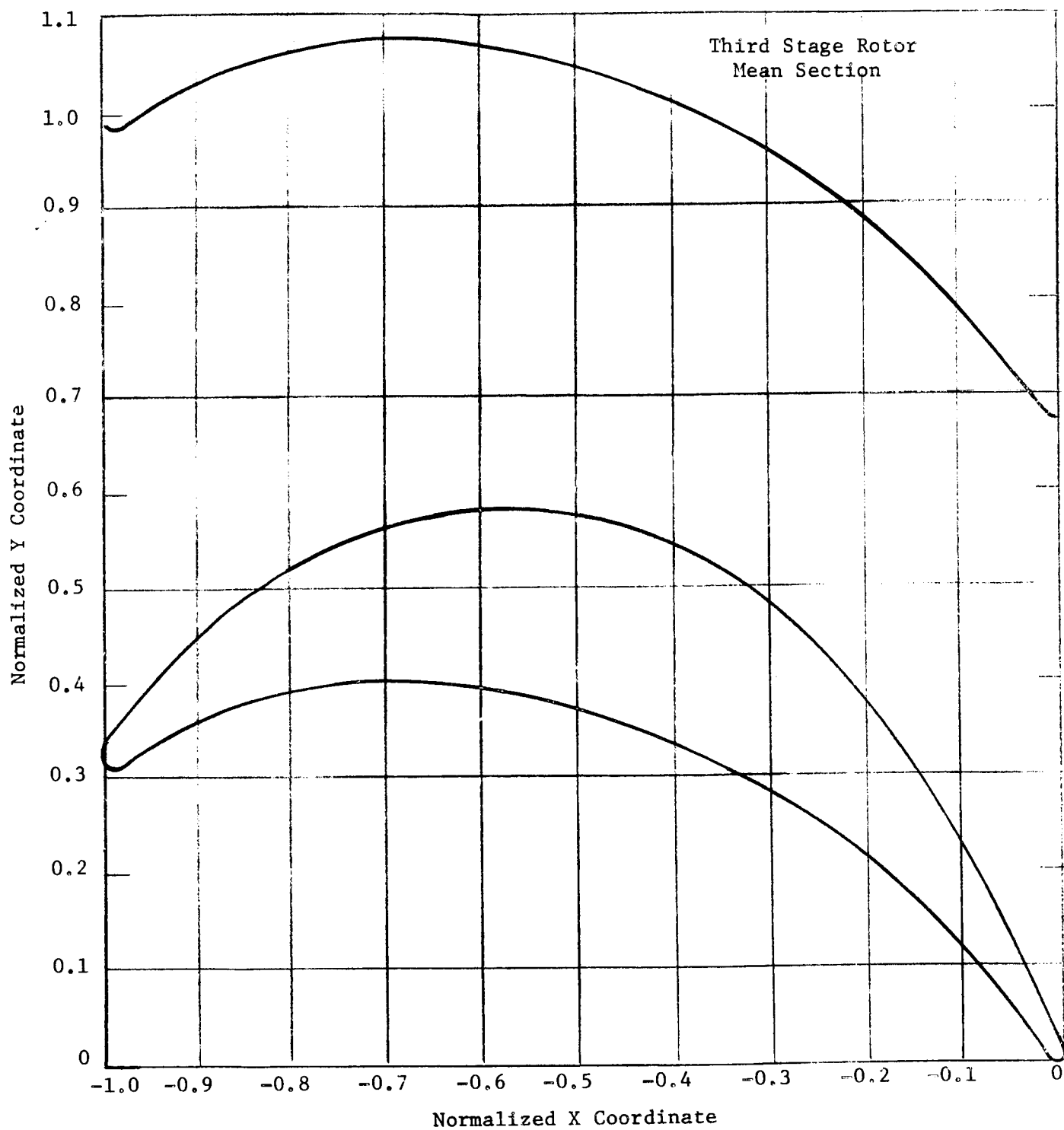
Figure 17. Third Stage Rotor Mean Section.
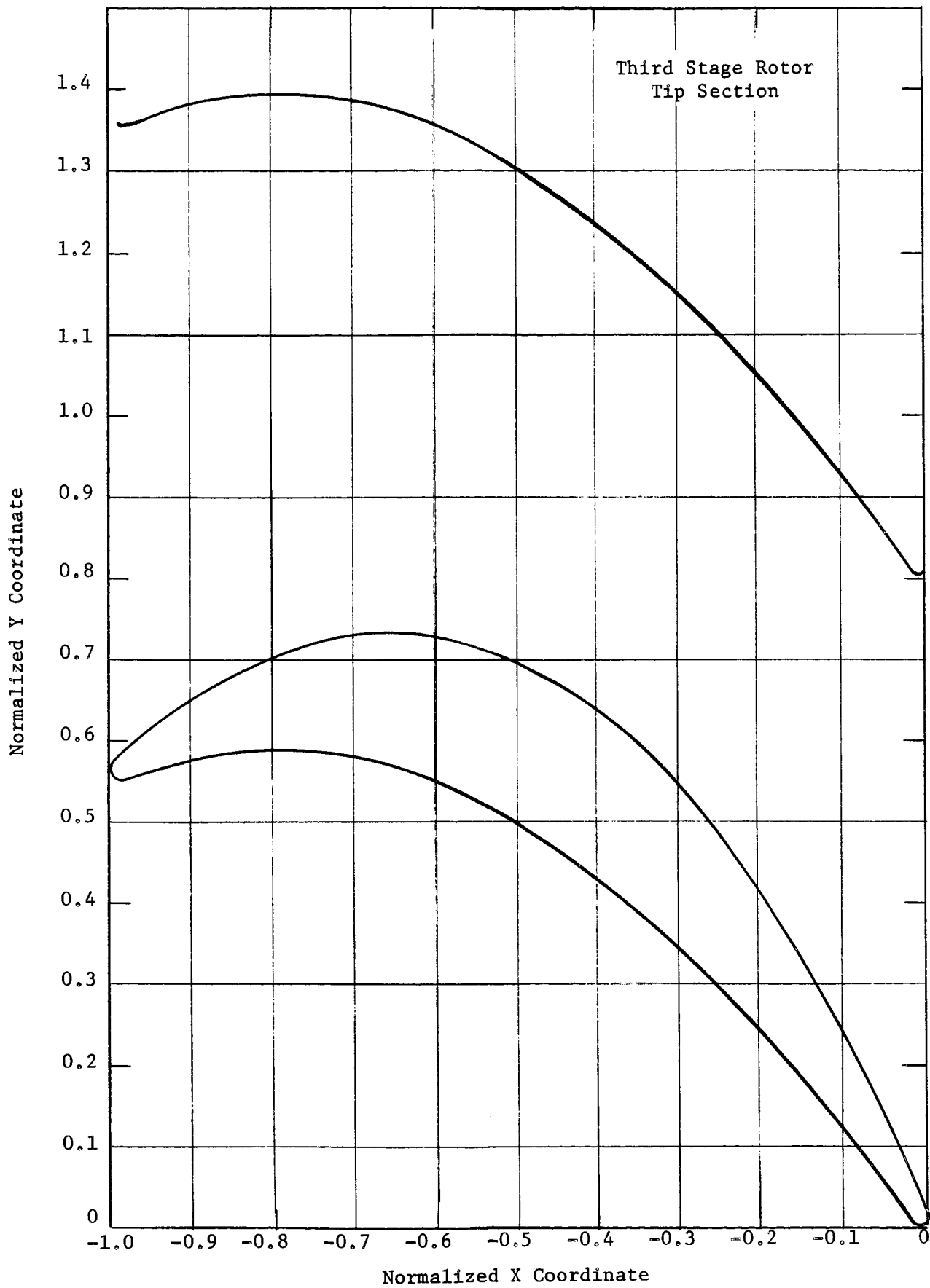
Figure 18. Third Stage Rotor Tip Section.
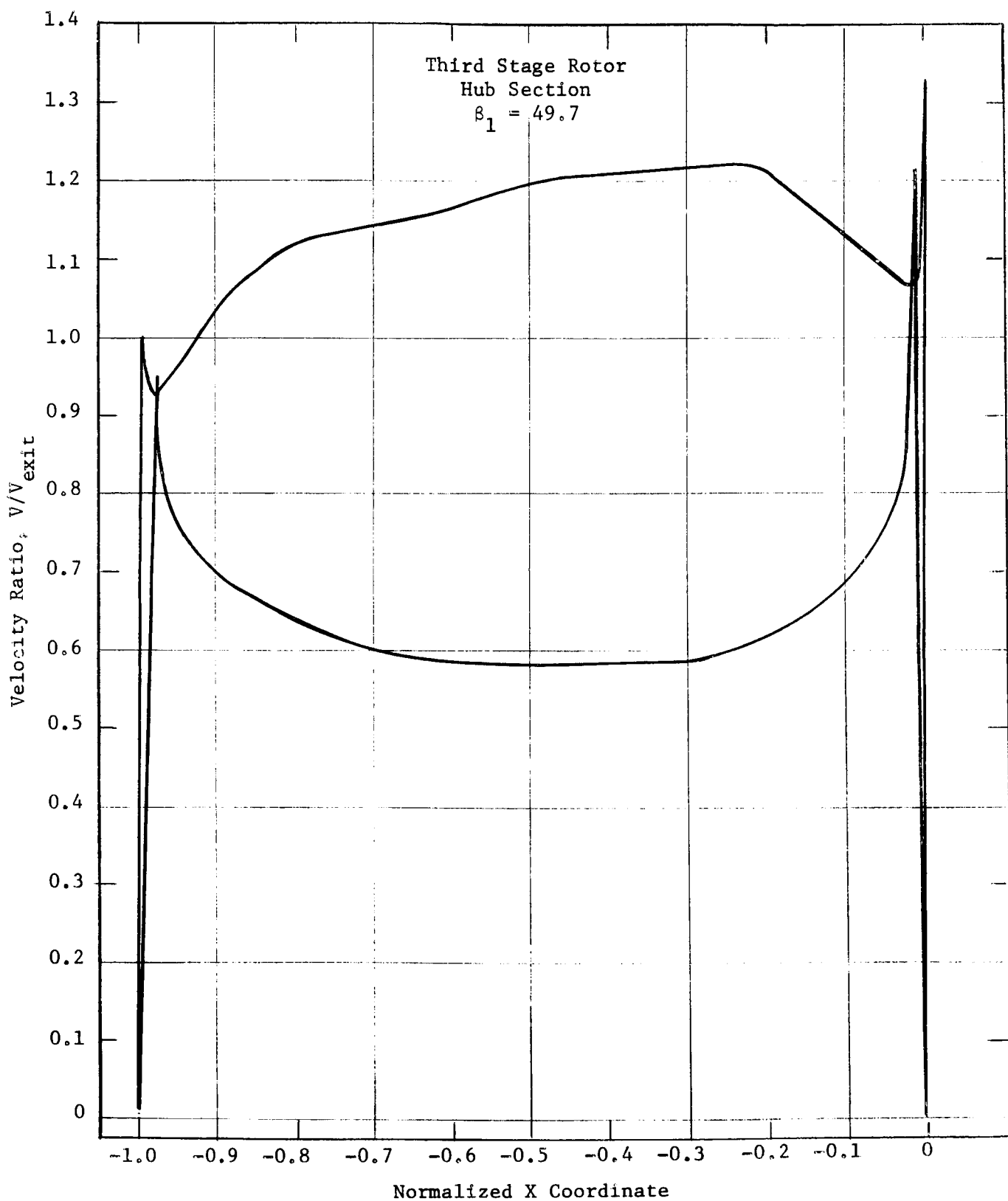
Figure 19. Third Stage Rotor Hub Section Velocity Distribution.
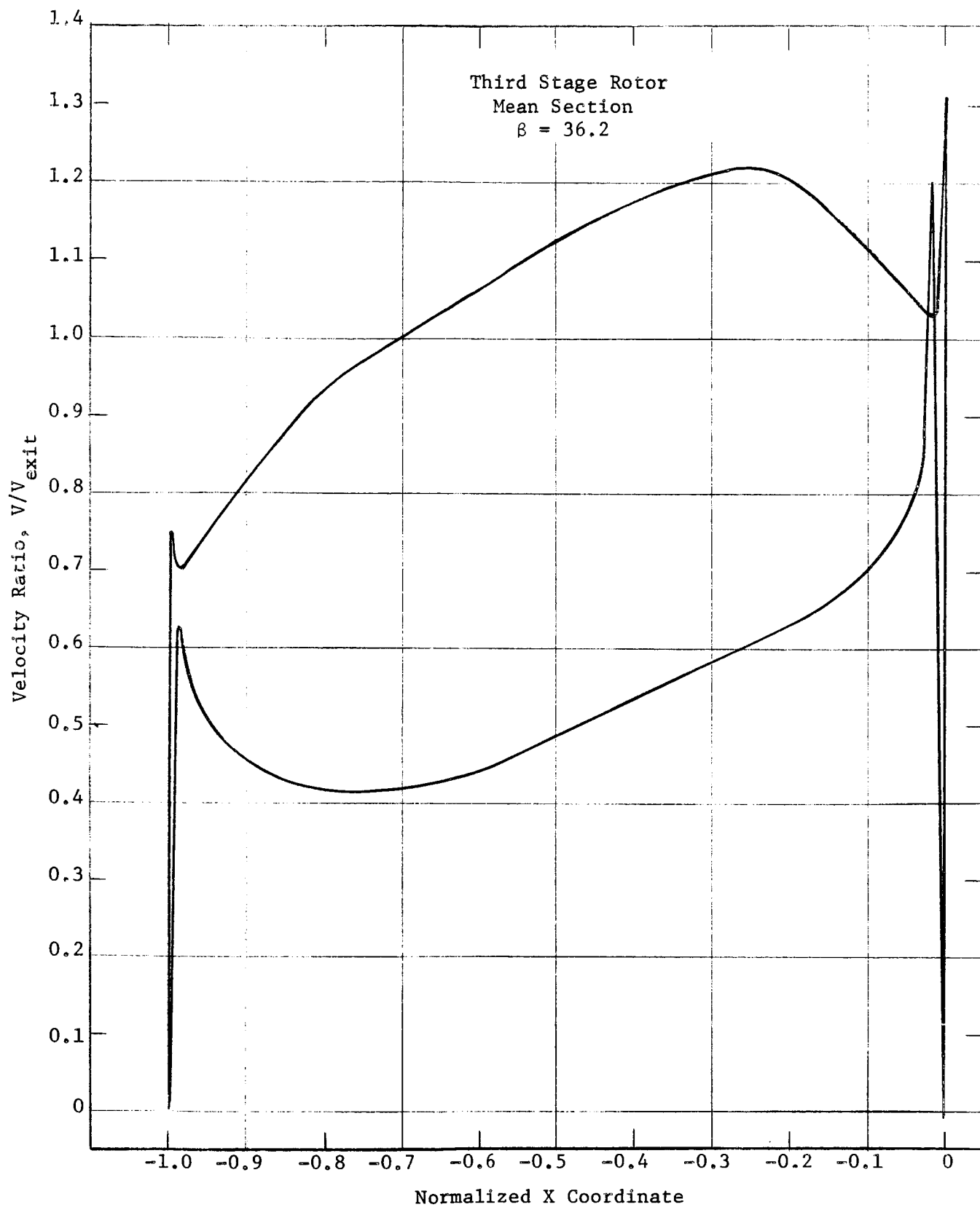
Figure 20. Third Stage Rotor Mean Section Velocity Distribution.
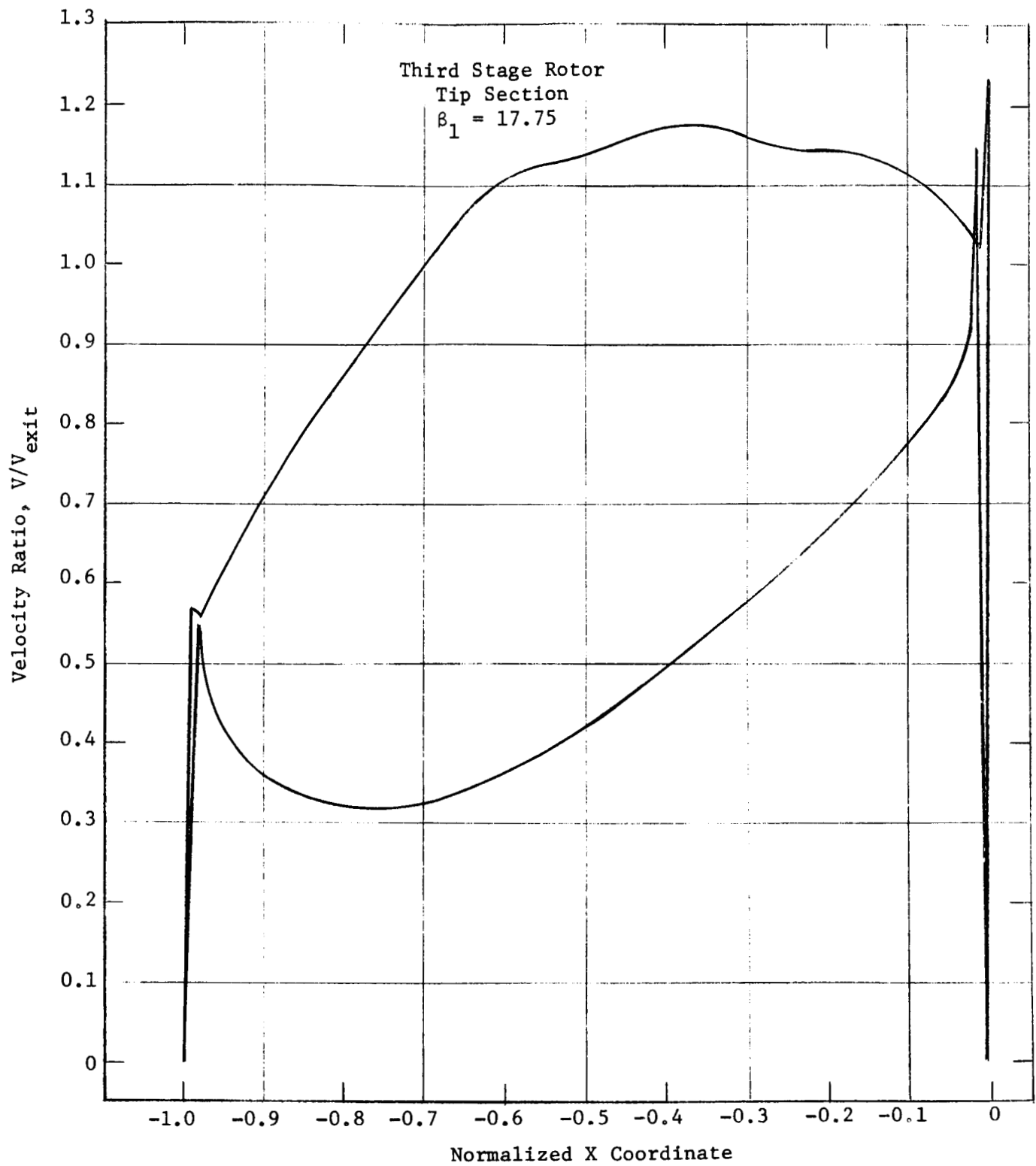
Figure 21.   Third Stage Rotor Tip Section Velocity Distribution.
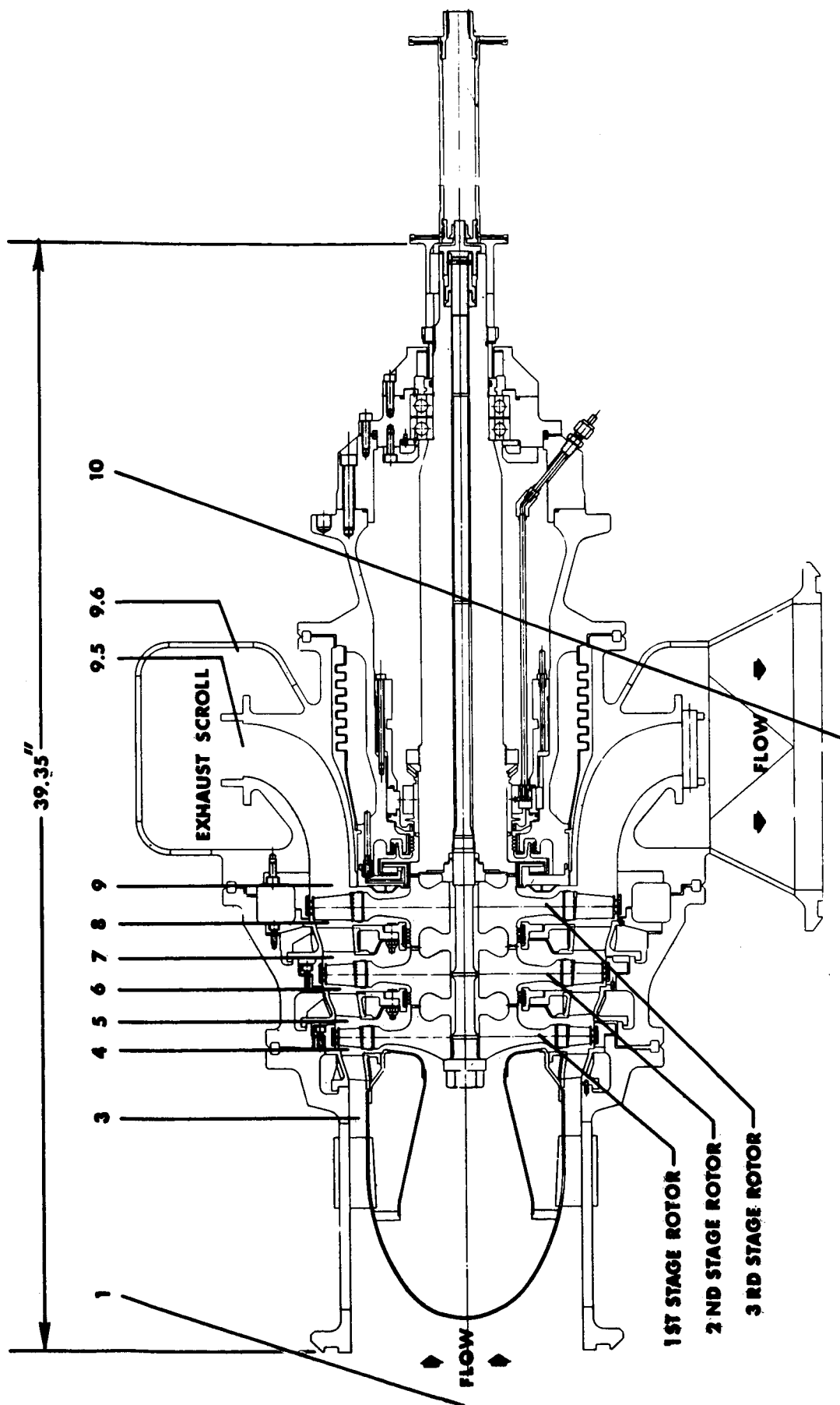
Figure 22   Instrumentation Stations.
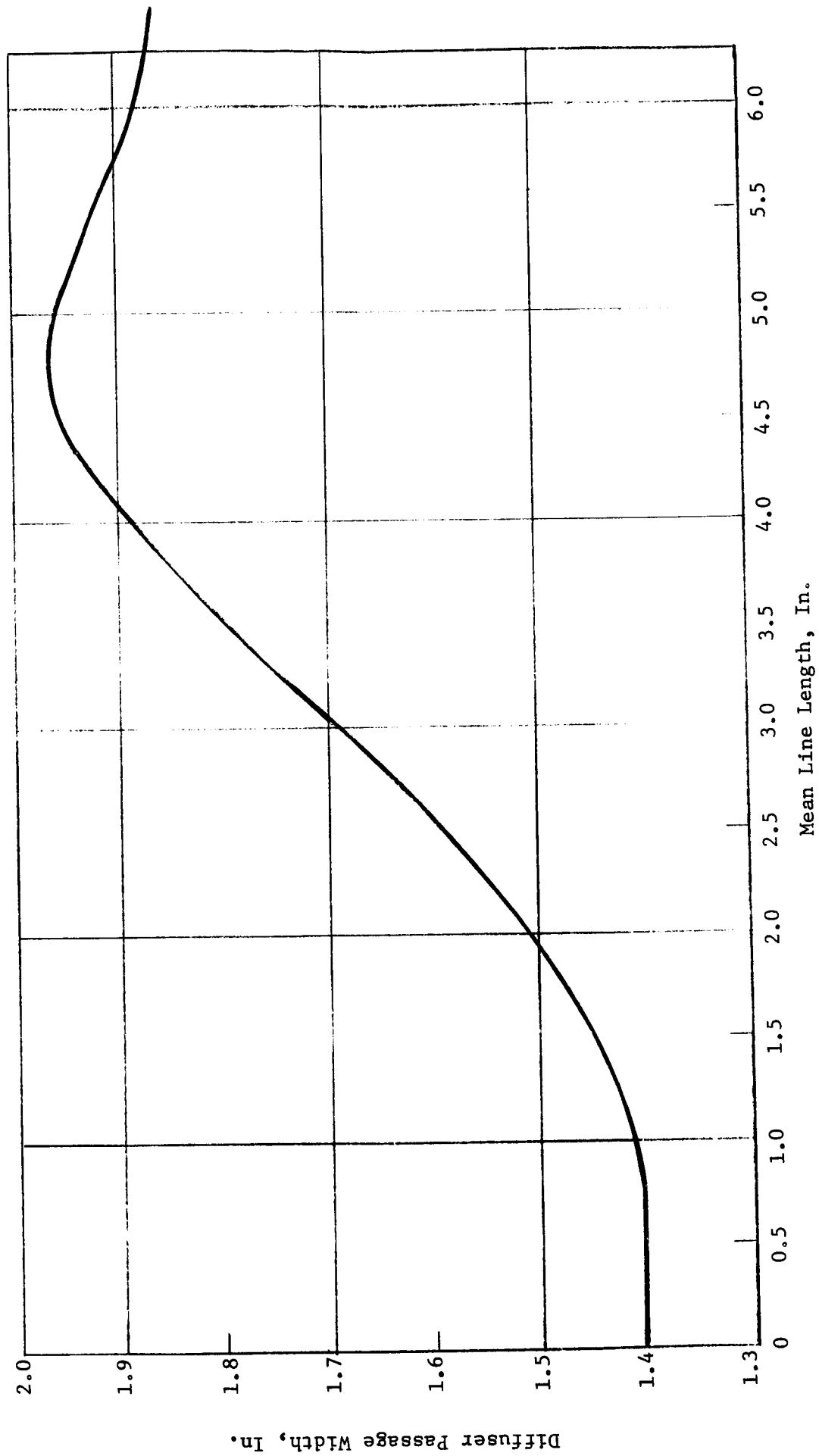
Figure 23. Diffuser Passage Width.
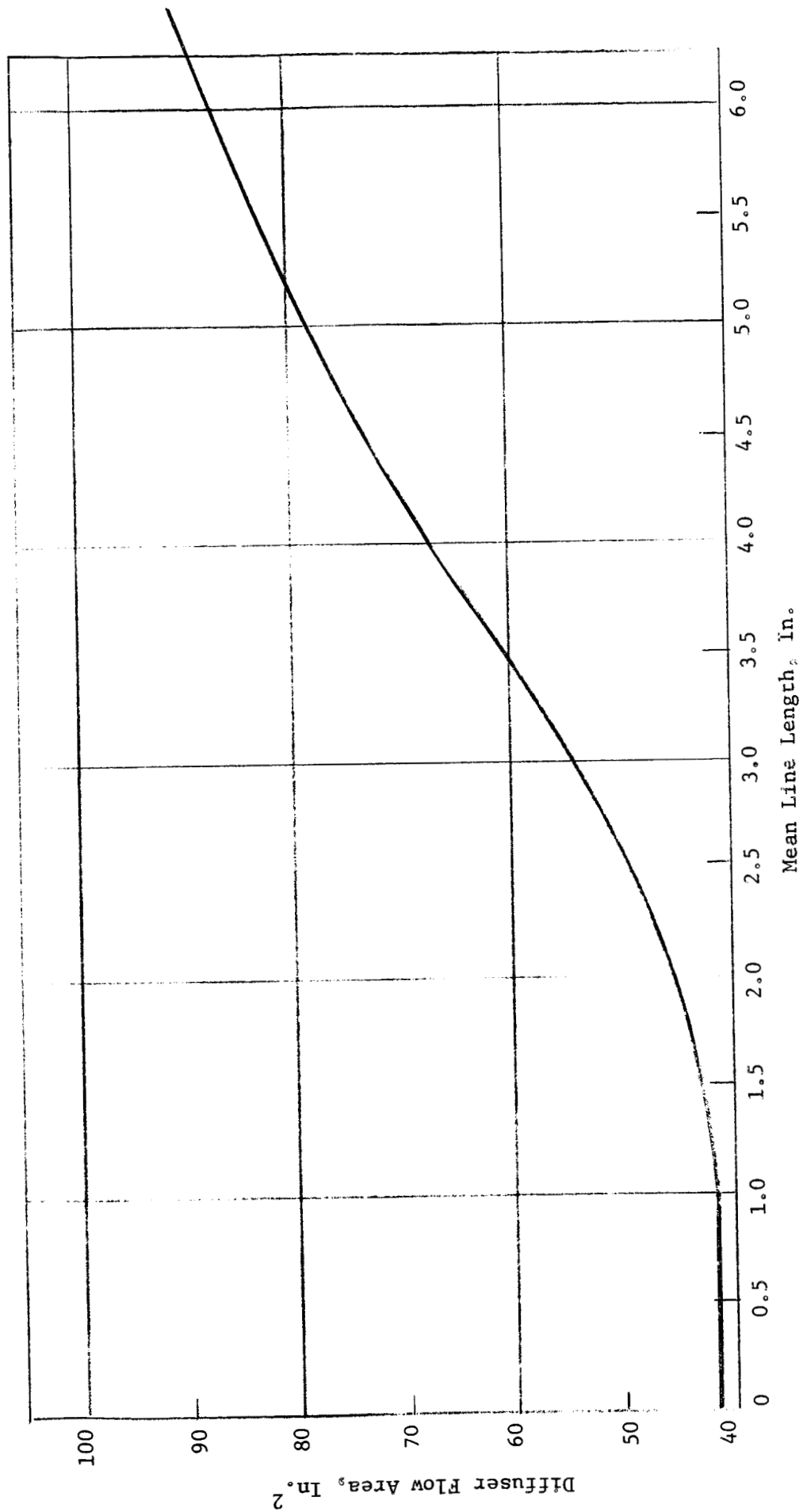
Figure 24. Diffuser Flow Area.
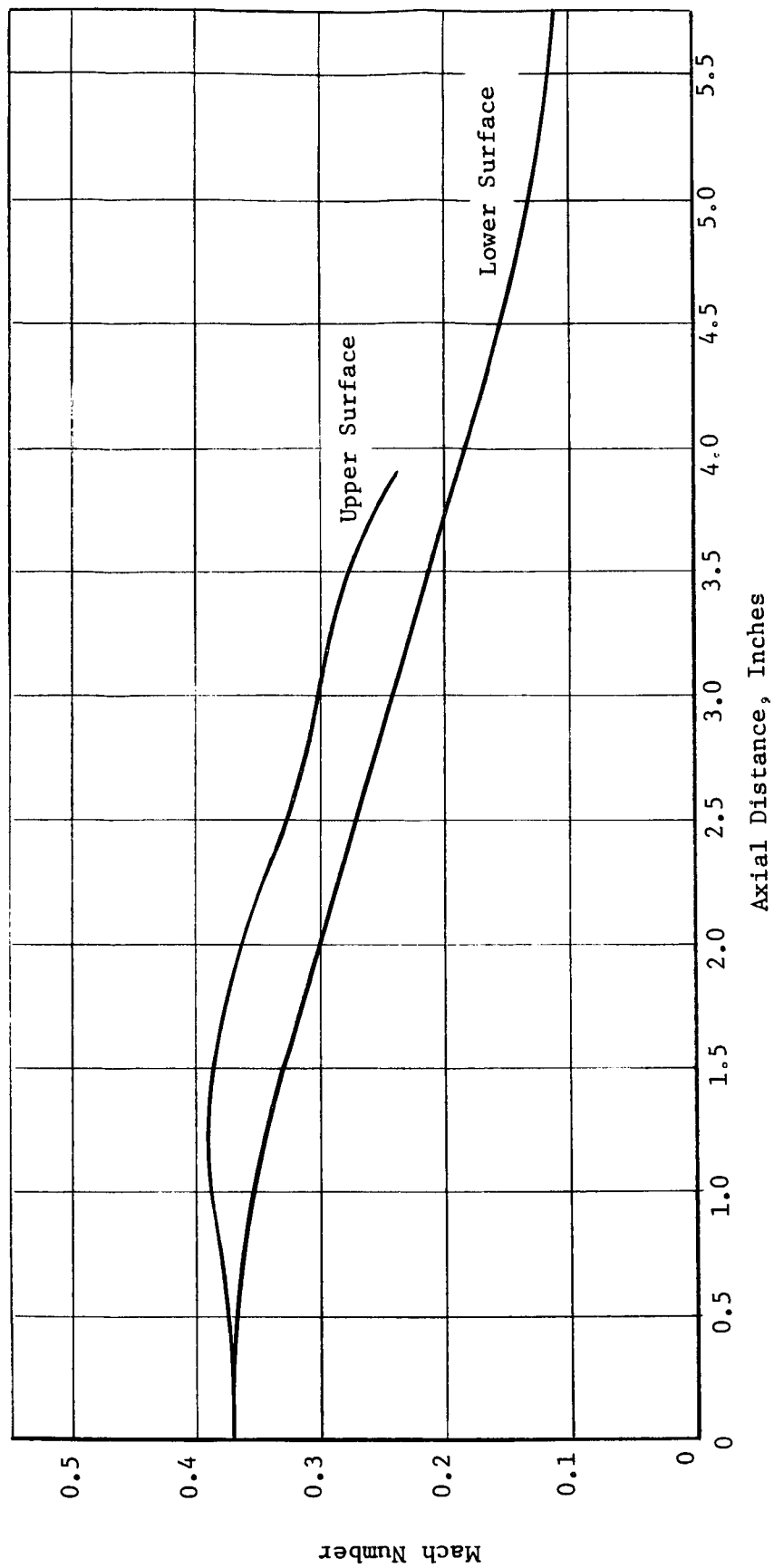
Figure 25. Exit Diffuser Surface Mach Numbers.

Upper Surface

Lower Surface

Mach Number

Axial Distance, Inches
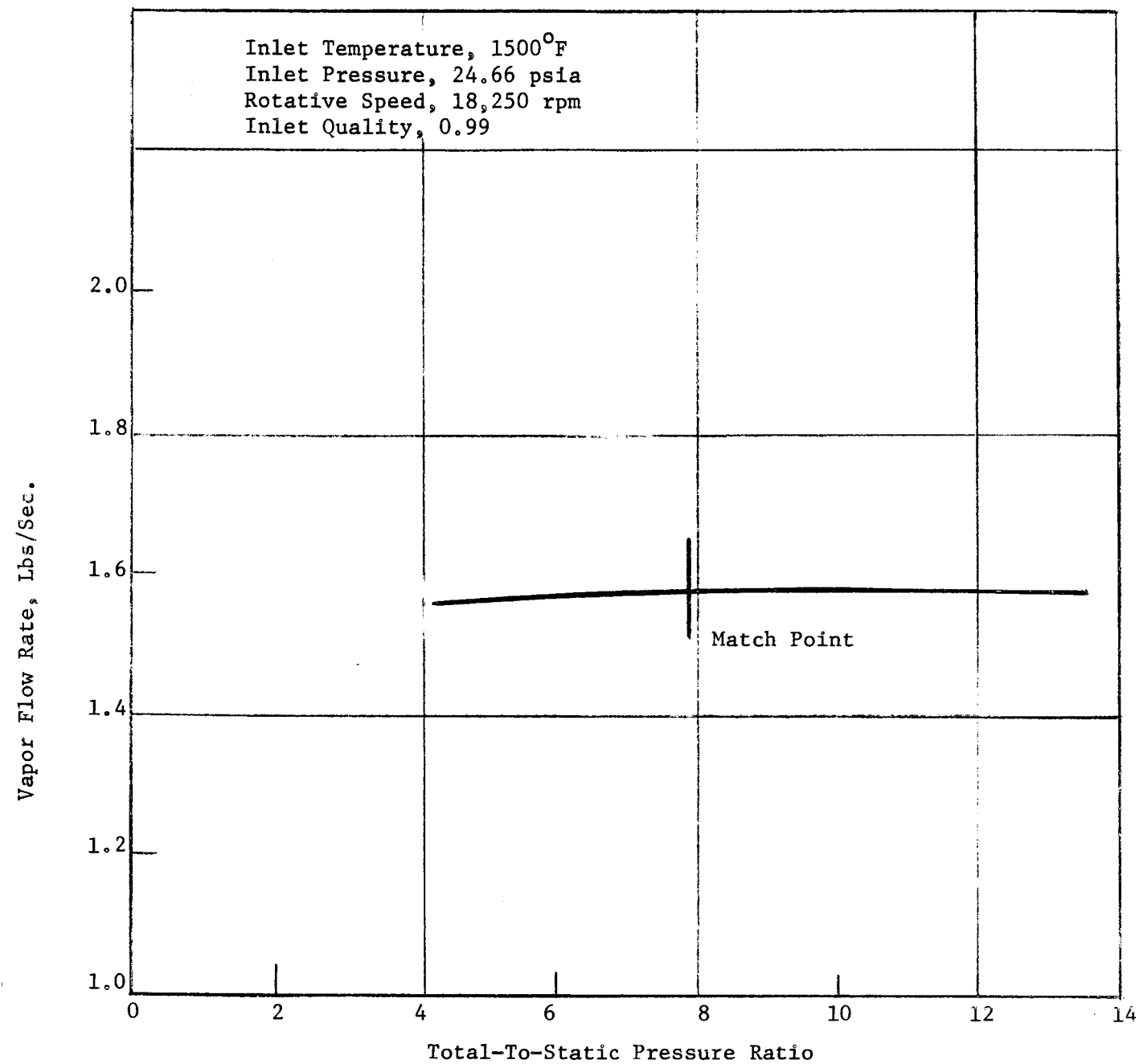
Figure 26. Three Stage-Turbine Vapor Flow Rate.
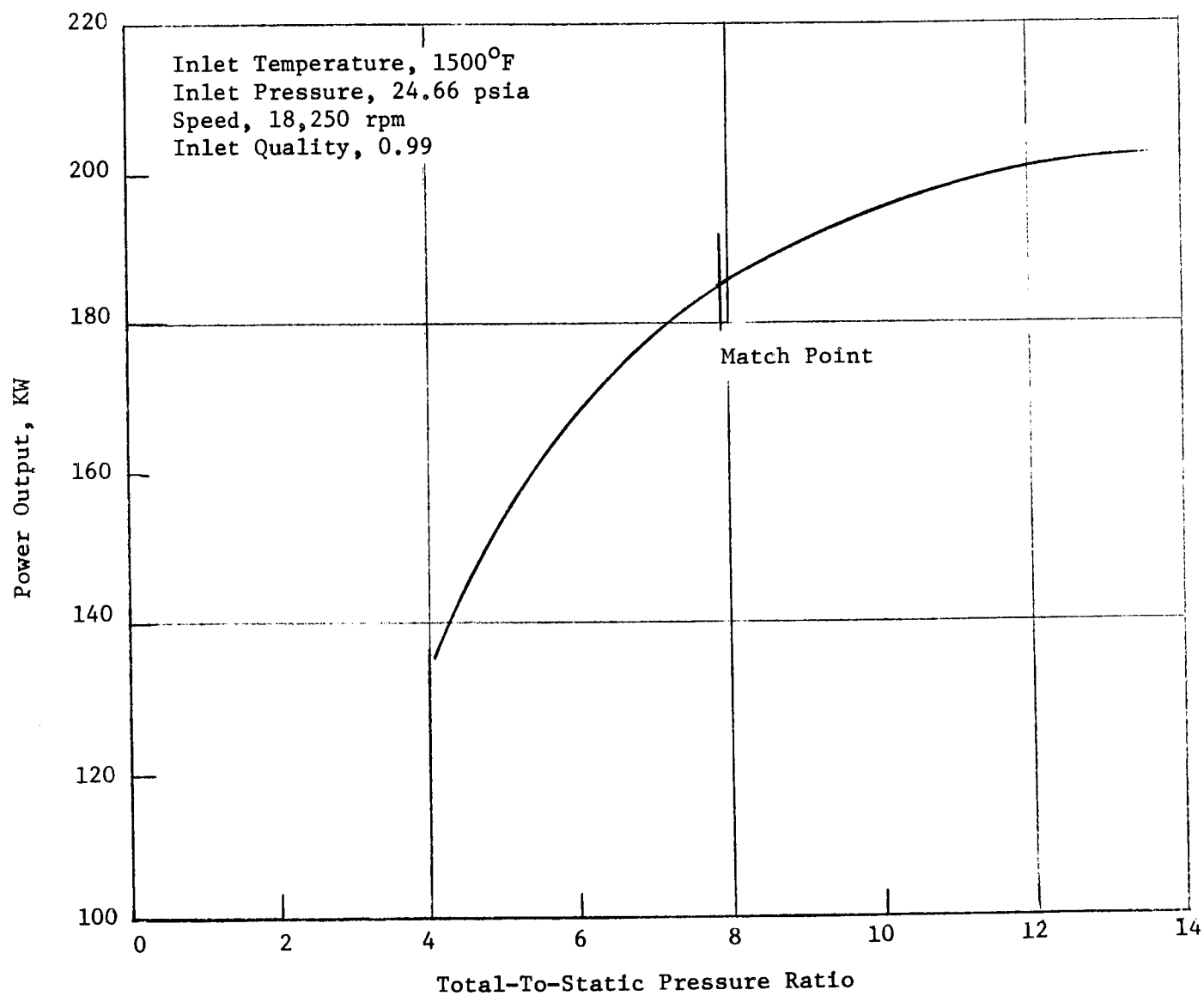
Figure 27. Three-Stage Turbine Power Output.
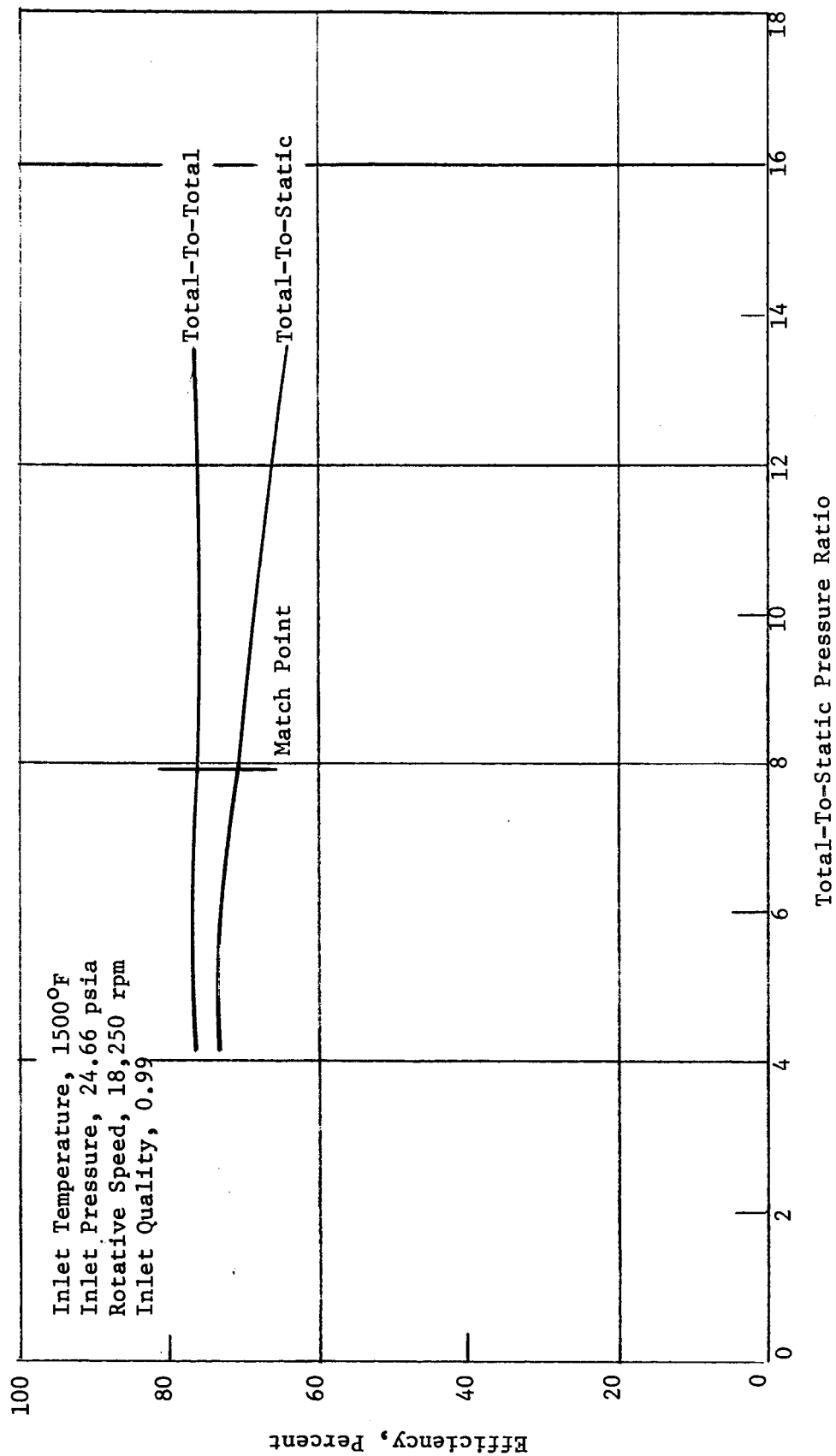
Figure 28. Three-Stage Turbine Efficiency.
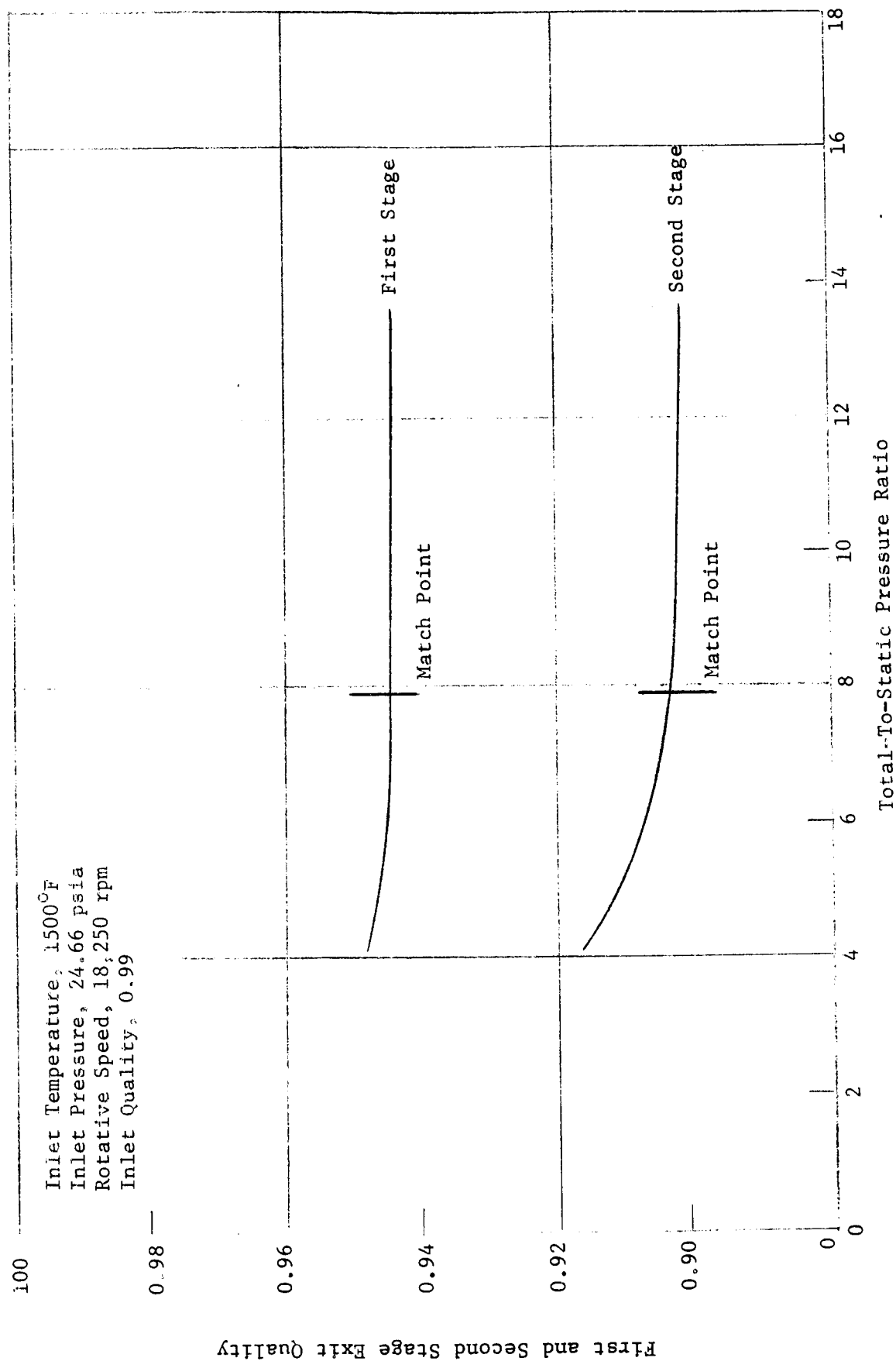
Figure 29. Vapor Quality of Three Stage Turbine.

Inlet Temperature, 1500°F
Inlet Pressure, 24.66 psia
Rotative Speed, 18,250 rpm
Inlet Quality, 0.99

First Stage

Second Stage

Match Point

Match Point

Total-To-Static Pressure Ratio

First and Second Stage Exit Quality
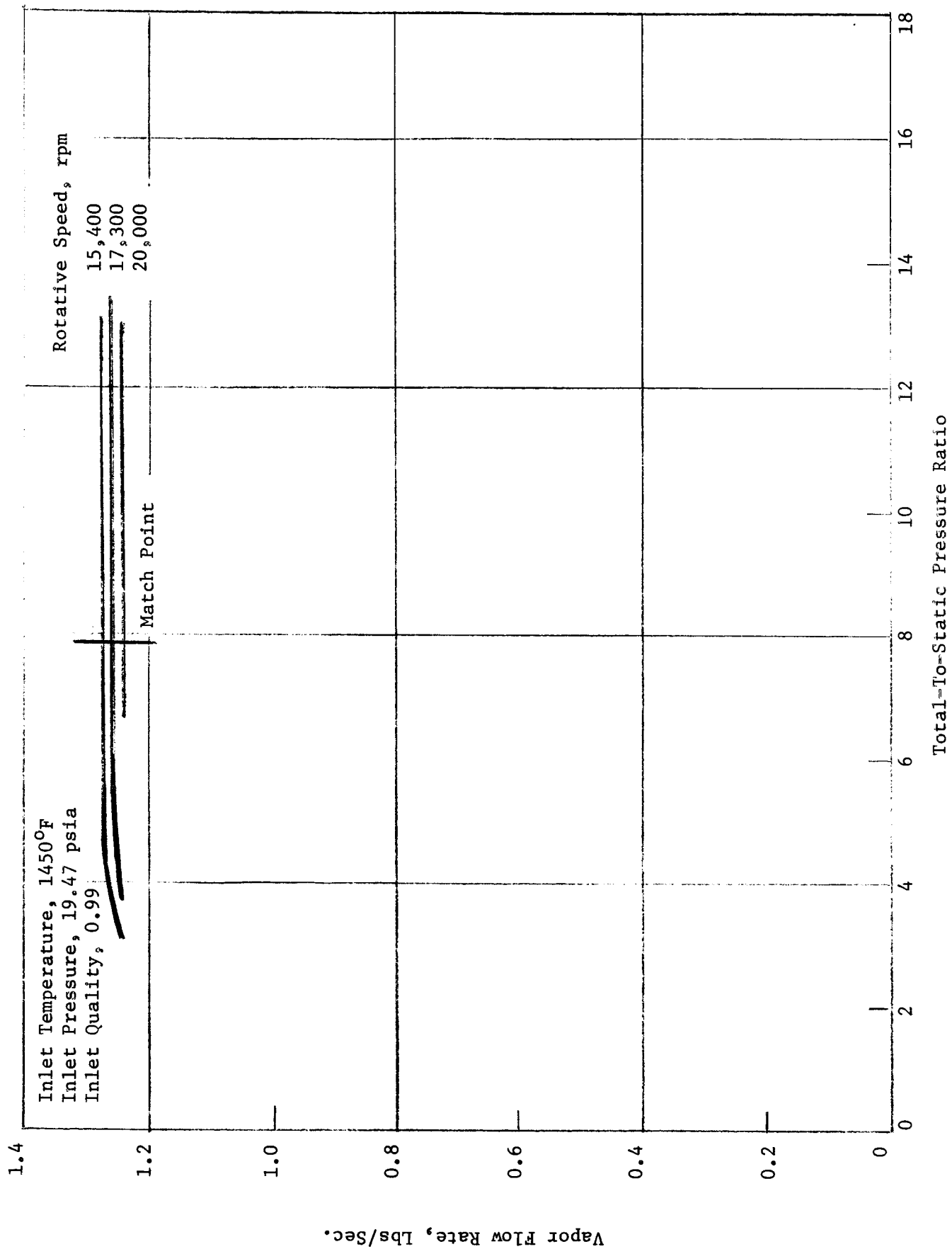
Figure 30. Three-Stage Turbine Vapor Flow Rate.
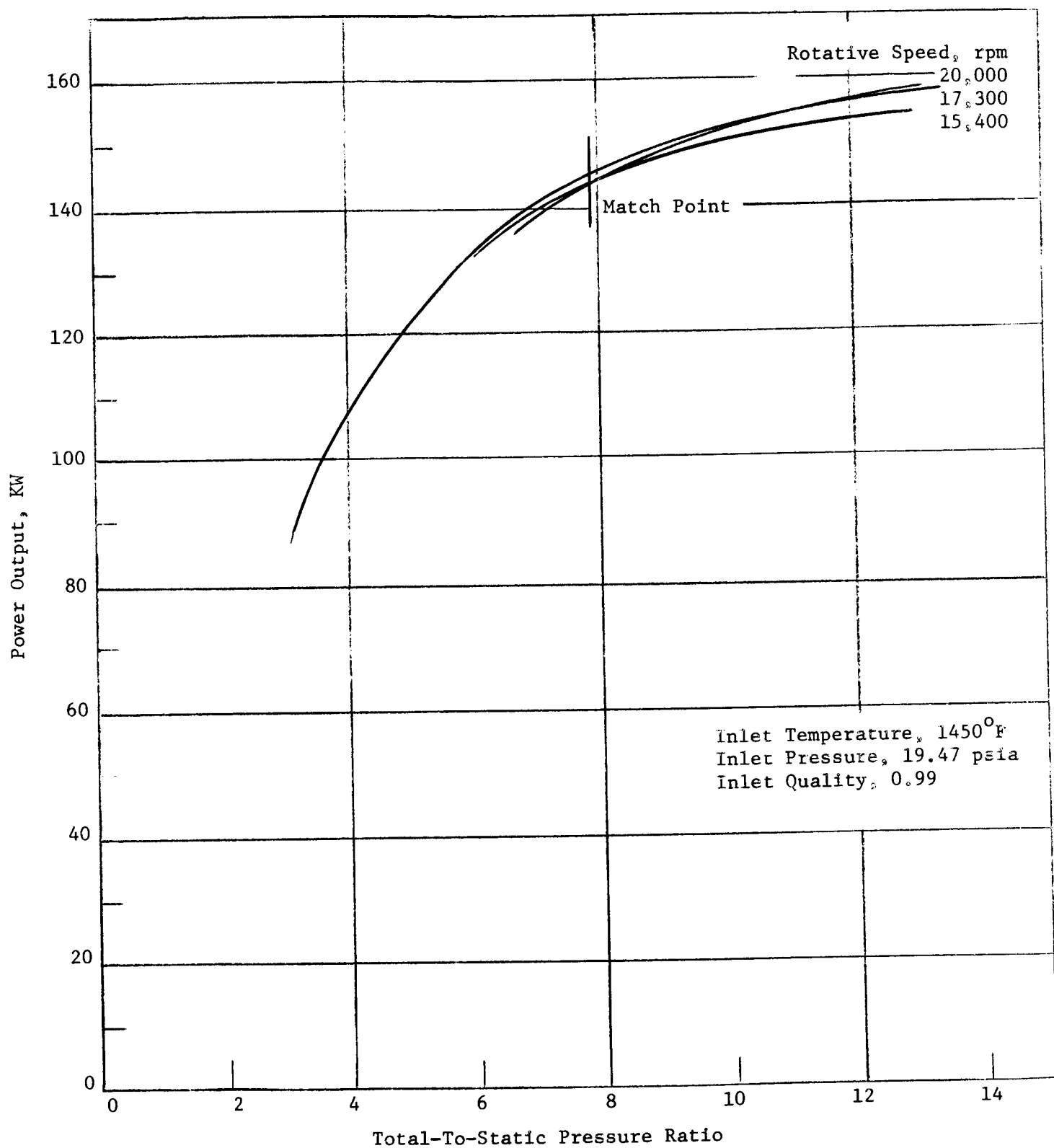
Figure 31. Three-Stage Turbine Power Output.
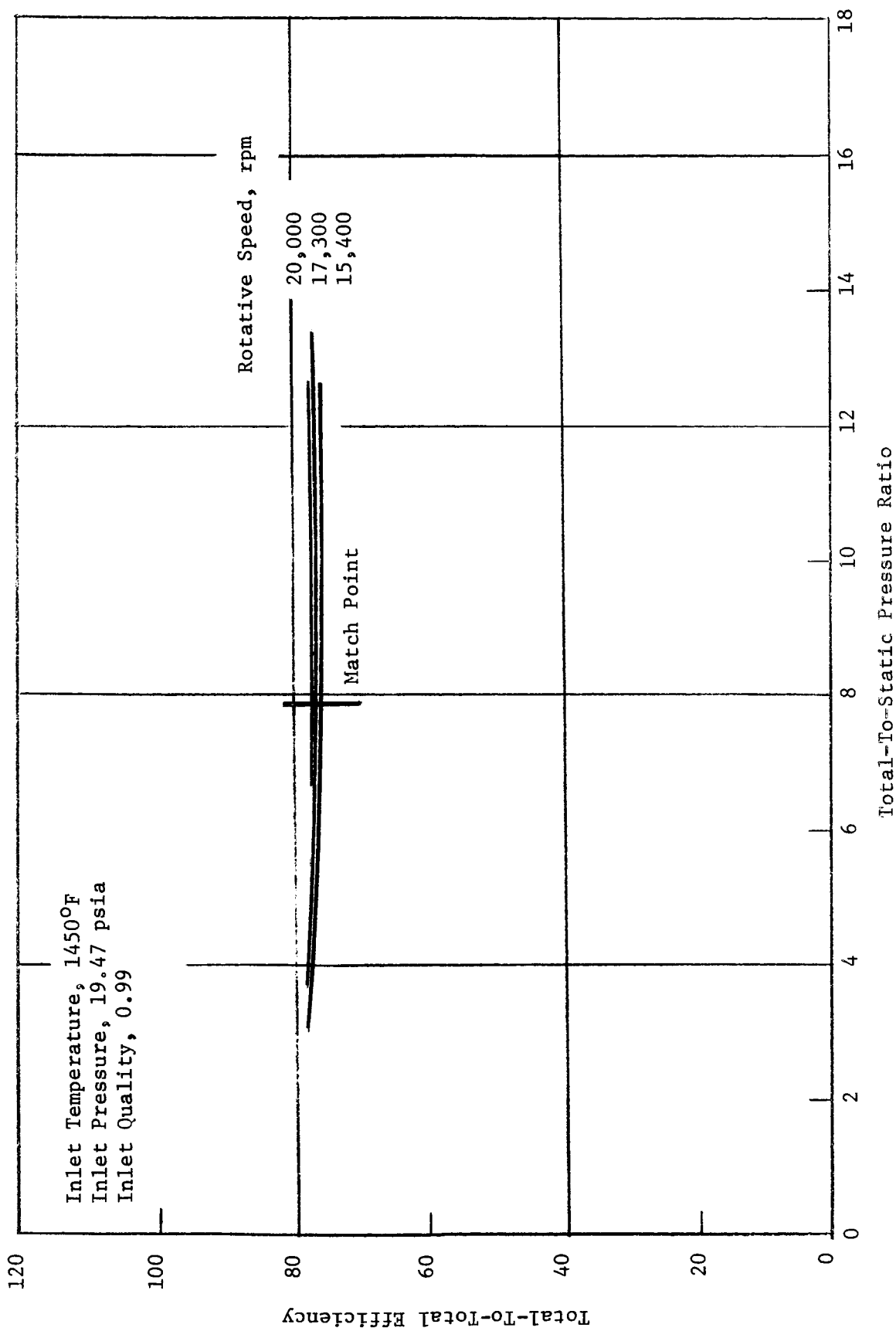
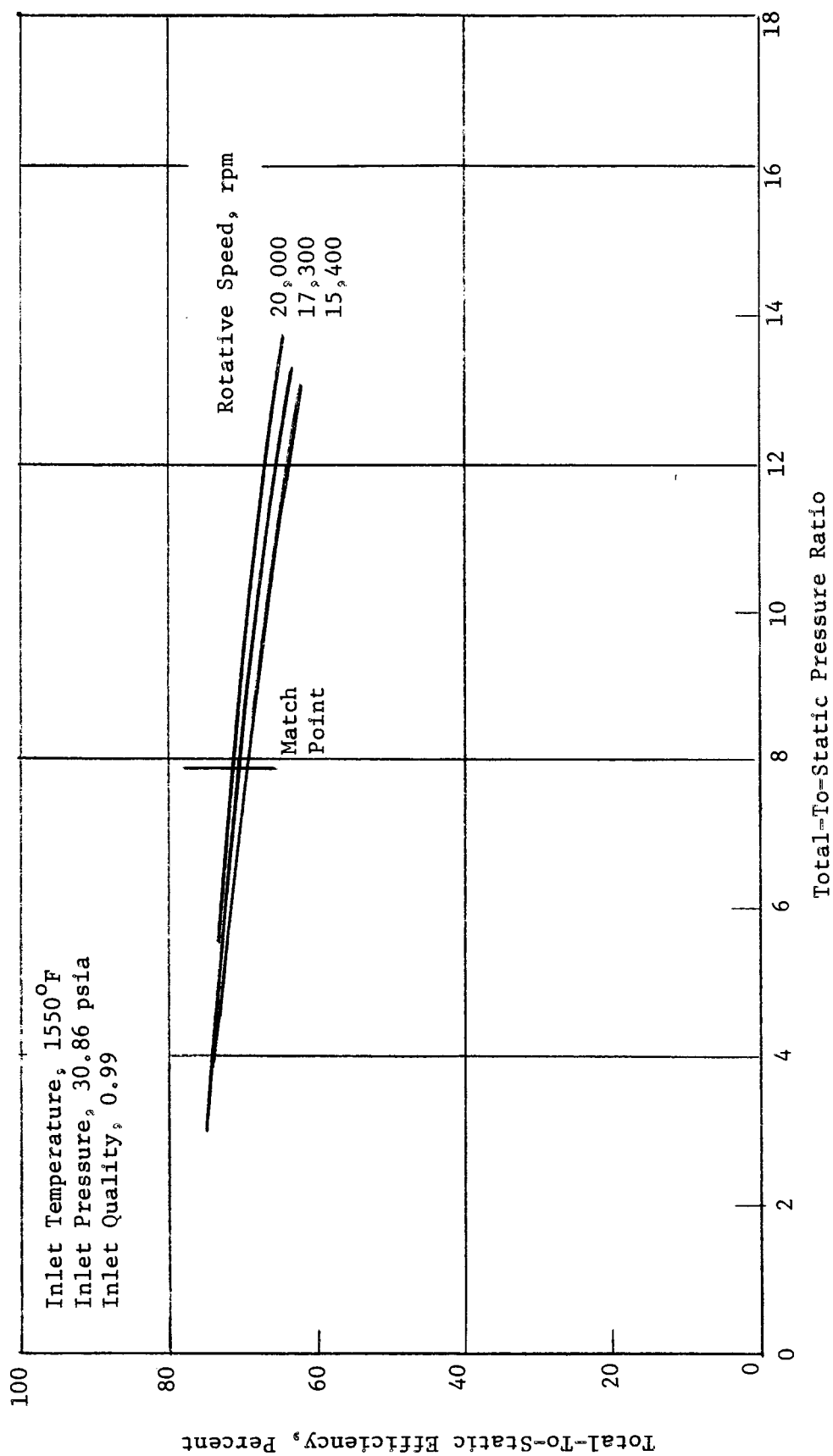Figure 32. Three-Stage Turbine Total-To-Total Efficiency.
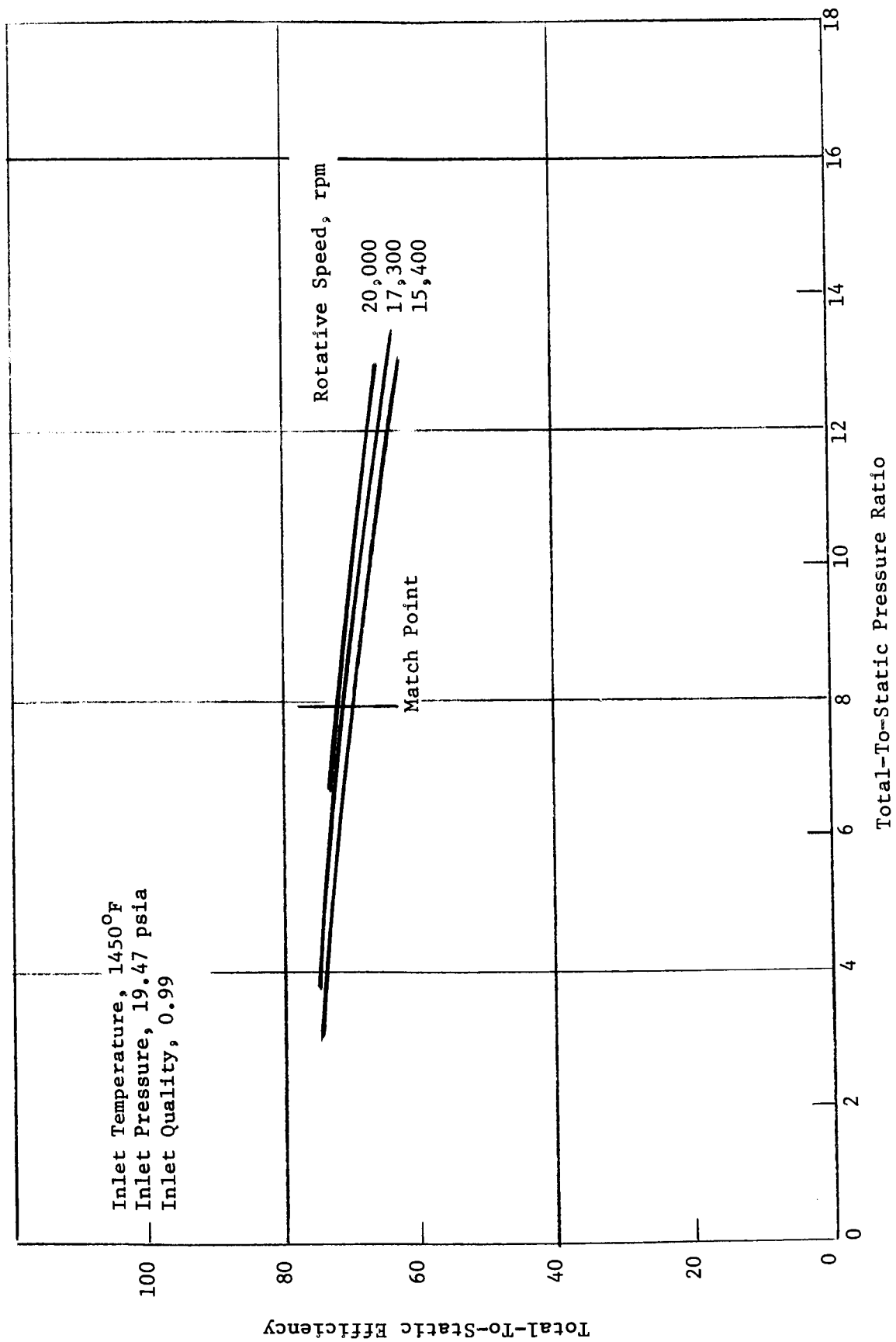
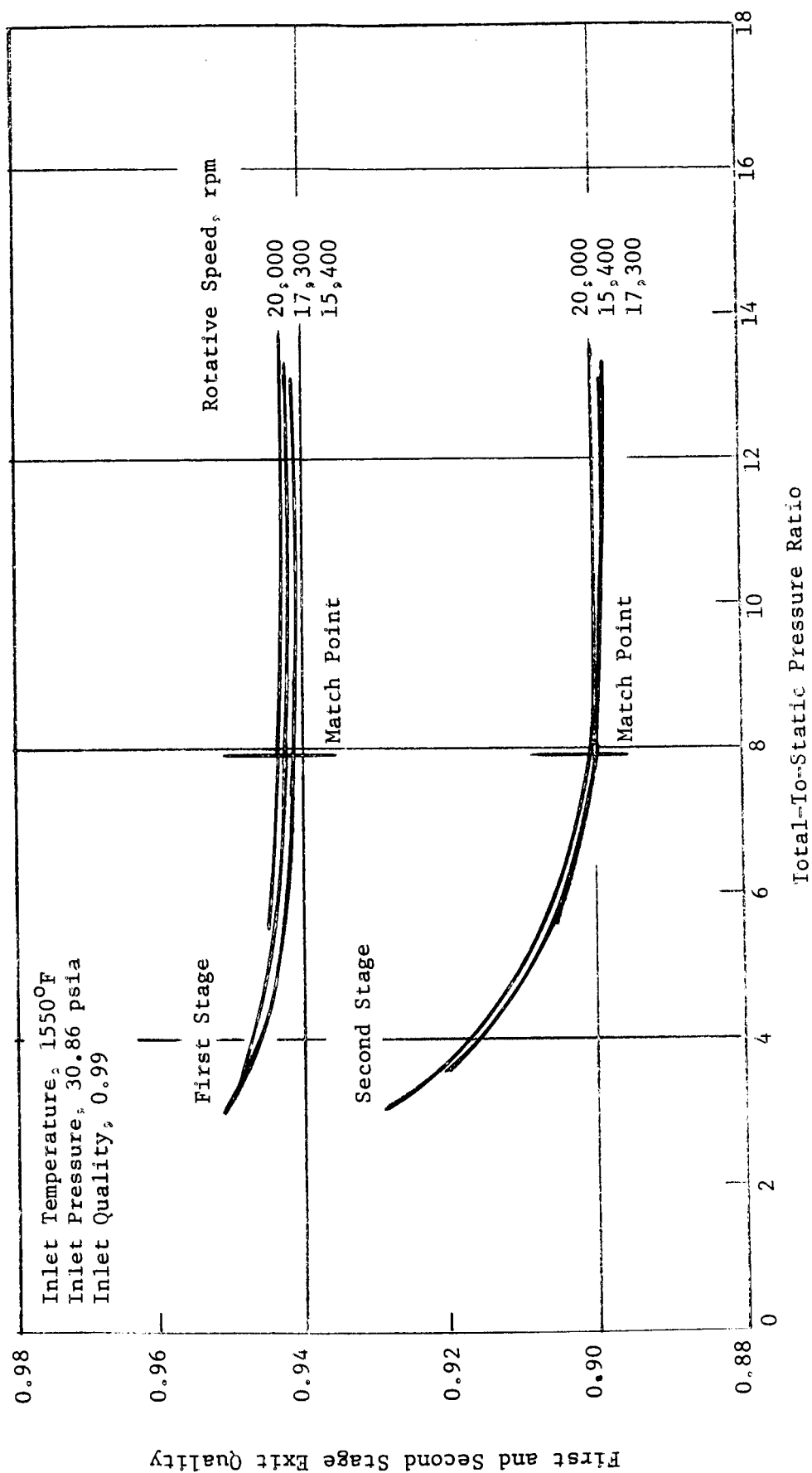Figure 33. Three-Stage Turbine Total-To-Static Efficiency.
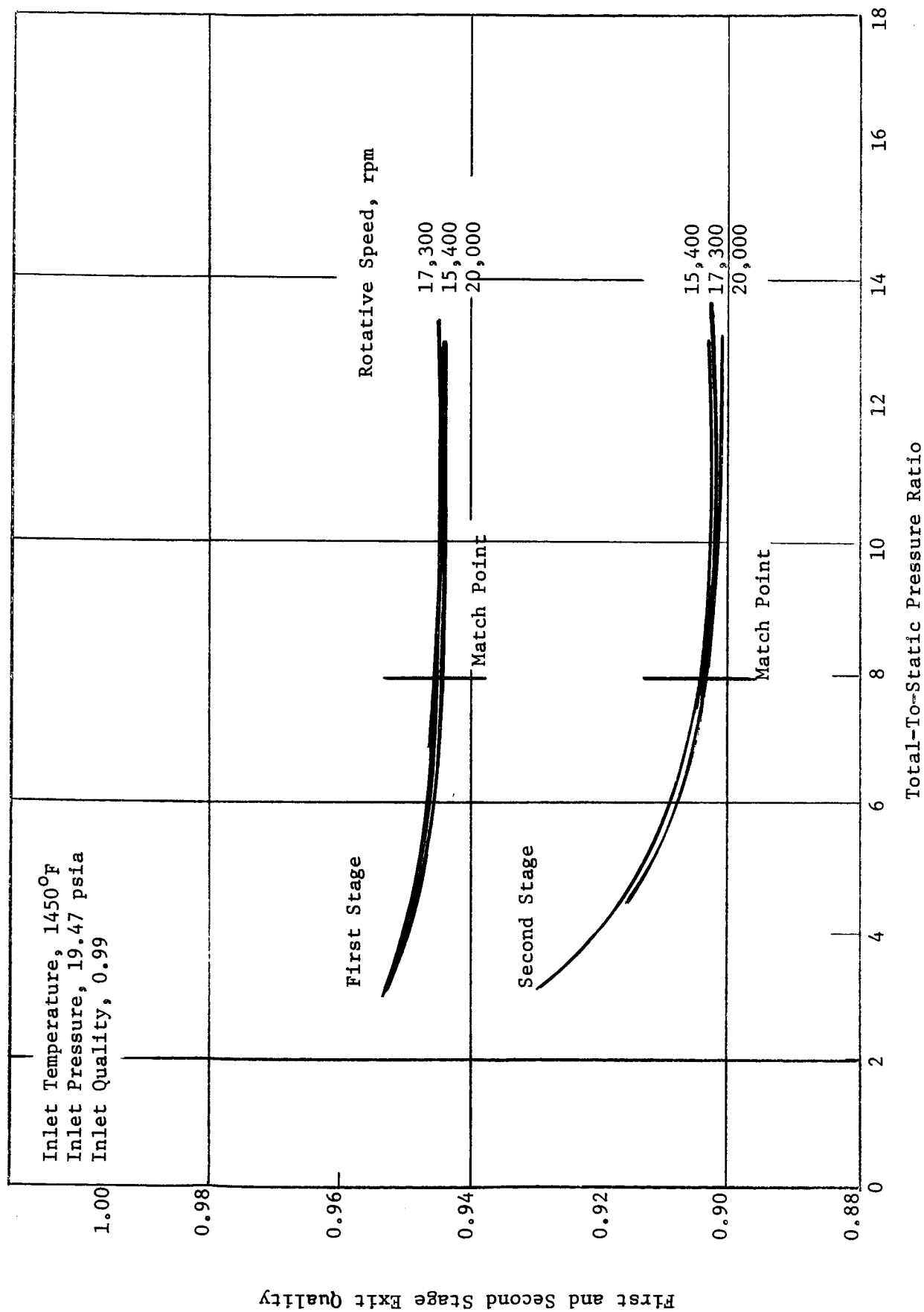
Figure 34. Vapor Quality of Three Stage Turbine.
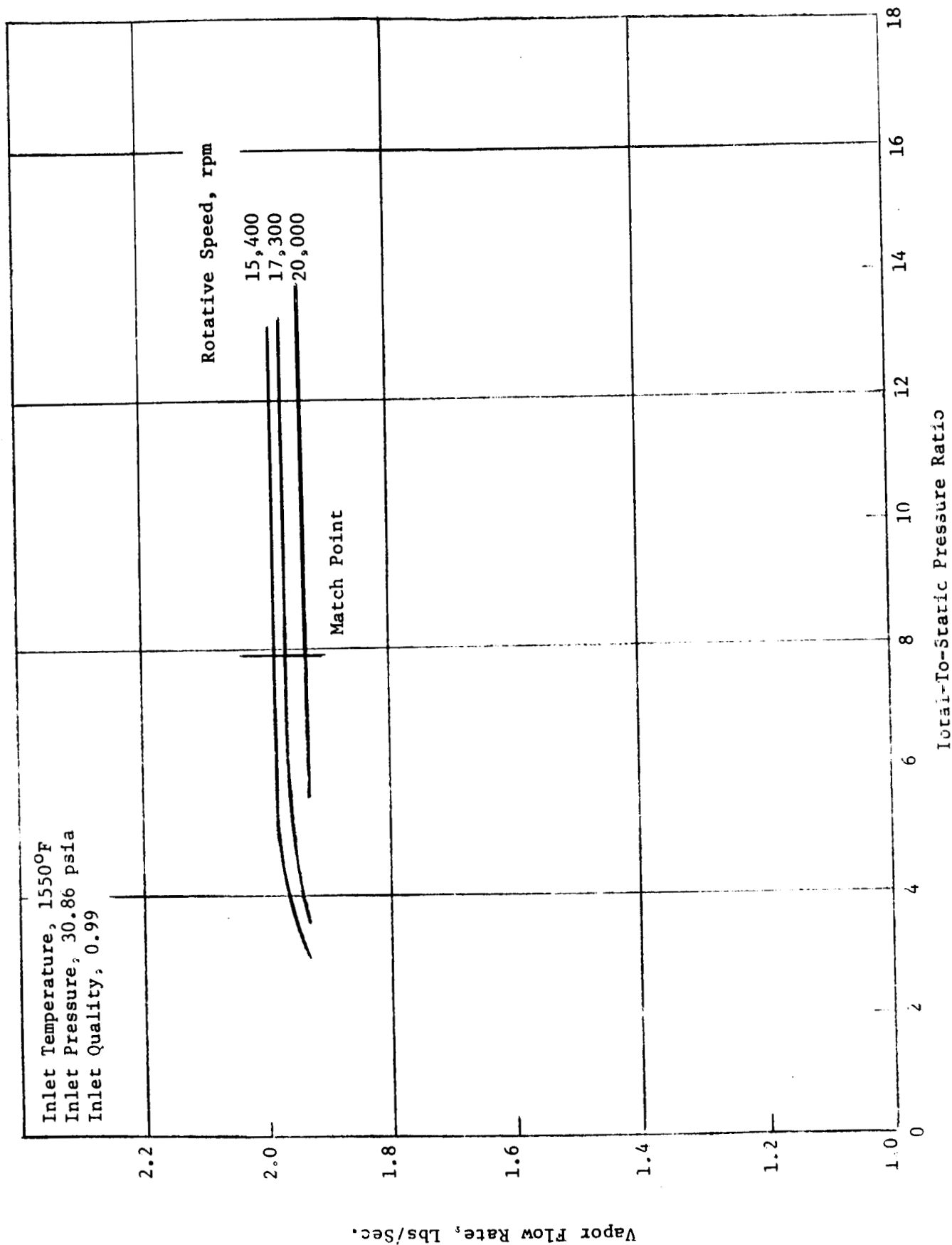
Figure 35. Three-Stage Turbine Vapor Flow Rate.
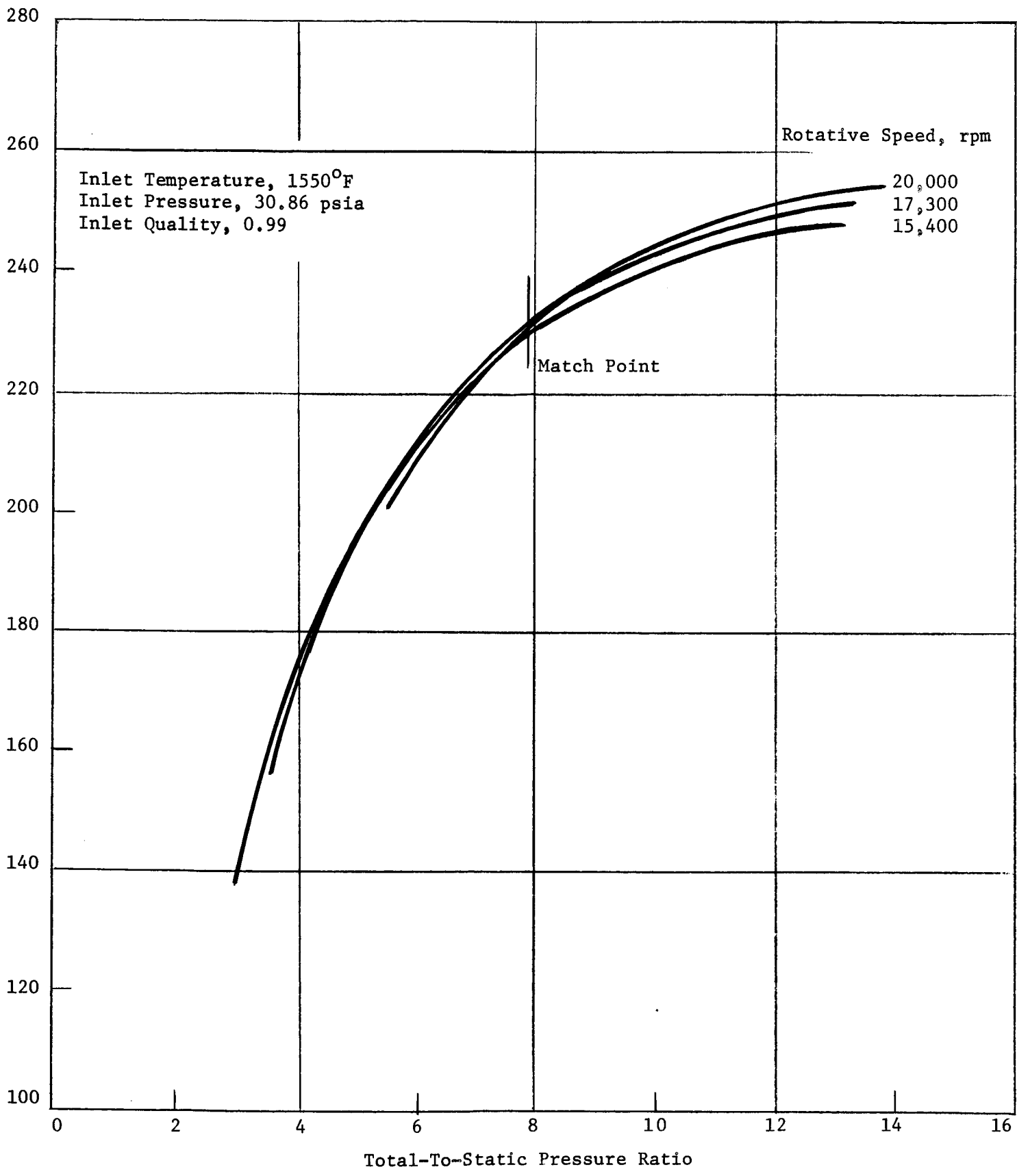
Figure 36. Three-Stage Turbine Power Output.
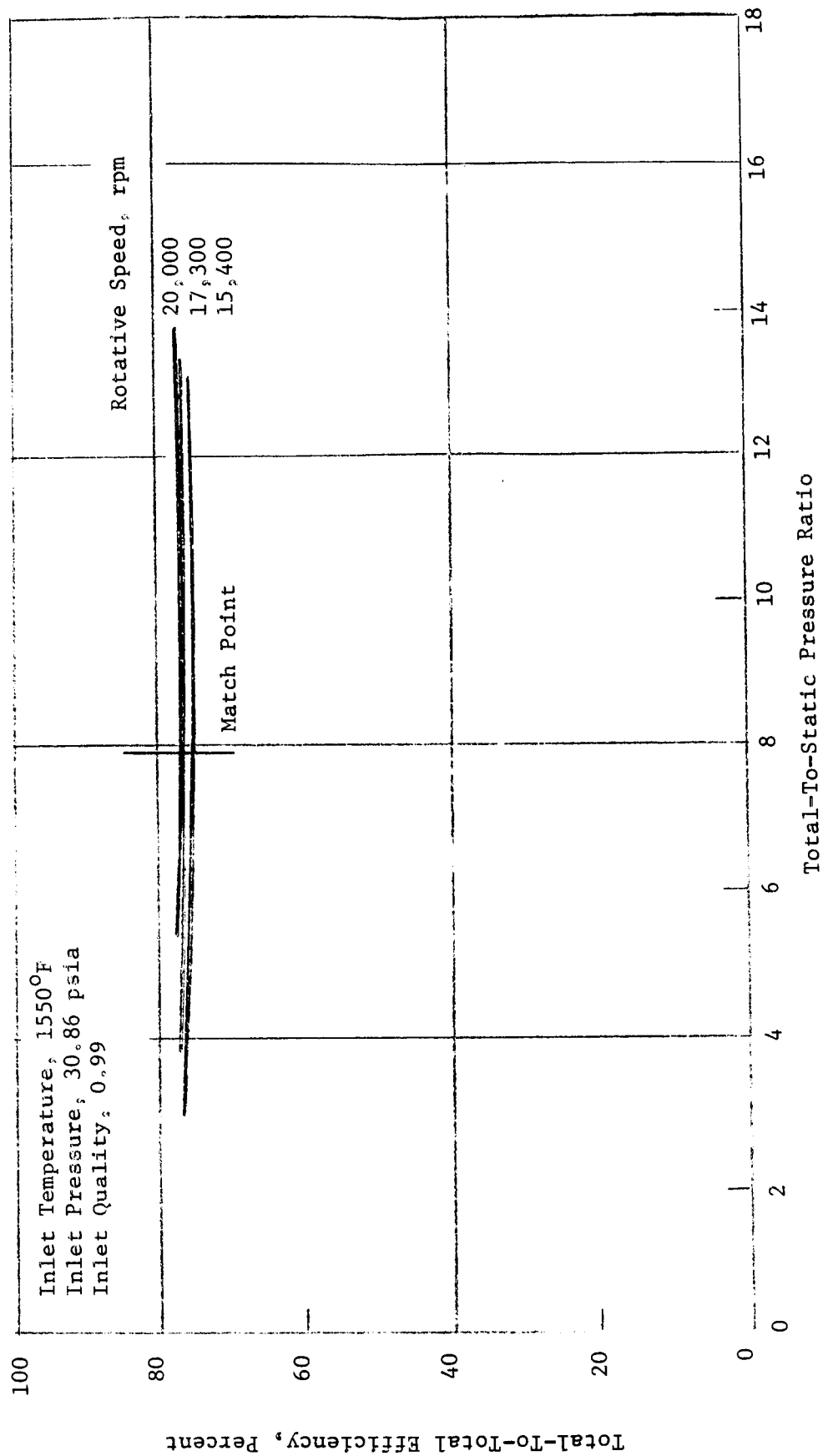
Figure 37. Three-Stage Turbine Total-To-Total Efficiency.

Figure 38. Three-Stage Turbine Total-To-Static Efficiency.

Figure 39. Vapor Quality of Three Stage Turbine.

National Aeronautics and Space Administration
Washington, D. C. 20546
Attn: W. H. Woodward (RN)

National Aeronautics and Space Administration
Washington, D. C. 20546
Attn: Dr. Fred Schulman (RNP)

National Aeronautics and Space Administration
Washington, D. C. 20546
Attn: J. J. Lynch (RNP)

National Aeronautics and Space Administration
Washington, D. C. 20546
Attn: S. V. Manson (RNP)

National Aeronautics and Space Administration
Washington, D. C. 20546
Attn: H. D. Rochen (RNP)

National Aeronautics and Space Administration
Scientific and Technical Information Facility
P. O. Box 33
College Park, Maryland 20740
Attn: Acquisition Branch (SQT-34054)
      (2 copies plus reproducible)

National Aeronautics and Space Administration
Lewis Research Center
21000 Brookpark Road
Cleveland, Ohio 44135
Attn: Dr. B. Lubarsky   MS 500-201

National Aeronautics and Space Administration
Lewis Research Center
21000 Brookpark Road
Cleveland, Ohio 44135
Attn: R. E. English   MS 500-201

National Aeronautics and Space Administration
Lewis Research Center
21000 Brookpark Road
Cleveland, Ohio 44135
Attn: T. A. Moss   MS 500-201

National Aeronautics and Space Administration
Lewis Research Center
21000 Brookpark Road
Cleveland, Ohio 44135
Attn: J. A. Heller   MS 500-201

National Aeronautics and Space Administration
Lewis Research Center
21000 Brookpark Road
Cleveland, Ohio 44135
Attn: J. P. Joyce   MS 500-201

National Aeronautics and Space Administration
Lewis Research Center
21000 Brookpark Road
Cleveland, Ohio 44135
Attn: H. O. Slone   MS 500-201

National Aeronautics and Space Administration
Lewis Research Center
21000 Brookpark Road
Cleveland, Ohio 44135
Attn: J. H. Dunn   MS 500-201

National Aeronautics and Space Administration
Lewis Research Center
21000 Brookpark Road
Cleveland, Ohio 44135
Attn: I. Pinkel   MS 5-3

National Aeronautics and Space Administration
Lewis Research Center
21000 Brookpark Road
Cleveland, Ohio 44135
Attn: W. L. Stewart   MS 77-2

National Aeronautics and Space Administration
Lewis Research Center
21000 Brookpark Road
Cleveland, Ohio 44135
Attn: J. E. Dilley   MS 500-309

National Aeronautics and Space Administration
Lewis Research Center
21000 Brookpark Road
Cleveland, Ohio 44135
Attn: T. P. Moffitt   MS 77-2

Distribution List For Final Report - Contract NAS 3-8520

National Aeronautics and Space Administration
Lewis Research Center
21000 Brookpark Road
Cleveland, Ohio 44135
Attn: N. Musial   MS 501-3

National Aeronautics and Space Administration
Lewis Research Center
21000 Brookpark Road
Cleveland, Ohio 44135
Attn: Library   MS 60-3 - 2 copies

National Aeronautics and Space Administration
Lewis Research Center
21000 Brookpark Road
Cleveland, Ohio 44135
Attn: Report Control Office   MS 5-5

National Aeronautics and Space Administration
Lewis Research Center
21000 Brookpark Road
Cleveland, Ohio 44135
Attn: P. E. Foster   MS 3-19

National Aeronautics and Space Administration
Lewis Research Center
21000 Brookpark Road
Cleveland, Ohio 44135
Attn: F. J. Dutee   MS 21-4

National Aeronautics and Space Administration
Lewis Research Center
21000 Brookpark Road
Cleveland, Ohio 44135
Attn: A. Glassman   MS 77-2

National Aeronautics and Space Administration
Lewis Research Center
21000 Brookpark Road
Cleveland, Ohio 44135
Attn: V. F. Hlavin   MS 3-14

LeRC/SNAP-8 Field Office
Aerojet-General Corporation
Von Karman Center
P. O. Box 754
Azusa, California 91702
Attn: J. G. Kennard

U. S. Atomic Energy Commission
Technical Information Service Extension
P. O. Box 62
Oak Ridge, Tennessee 37831

U. S. Atomic Energy Commission
Washington, D. C. 20545
Attn: Dr. Nicholas Grossman

U. S. Atomic Energy Commission
Washington, D. C. 20545
Attn: Lt. Col. G. M. Anderson

Aerojet-General Corporation
Von Karman Center
P. O. Box 296
Azusa, California 91702
Attn: Paul I. Wood

Atomics International
North American Aviation, Inc.
P. O. Box 309
Canoga Park, California 91304
Attn: R. W. Dickinson

Battelle Memorial Institute
505 King Avenue
Columbus, Ohio 43201
Attn: C. M. Allen

Brookhaven National Laboratory
Upton, Long Island, New York 11973
Attn: Dr. O. E. Dwyer

Curtiss-Wright Corporation
Wright-Aeronautical Division
Wood Ridge, New Jersey 07075
Attn: S. Lombardo

Defense Documentation Center
Cameron Station
Alexandria, Virginia 22314

Ford Motor Company
Aeronutronic Division
Ford Road
Newport Beach, California 92660
Attn: George P. Carver

Distribution List For Final Report - Contract NAS 3-8520

Ford Motor Company
Aeronutronic Division
Ford Road
Newport Beach, California 92660
Attn: Hans D. Linhardt

The Franklin Institute
Benjamin Framklin Parkway @ 20th St.
Philadelphia, Pennsylvania 19103
Attn: Otto Decker

The Garrett Corporation
AiResearch Mfg. Company
Phoenix, Arizona 85034
Attn: Robert Gruntz

The Garrett Corporation
AiResearch Mfg. Company
Phoenix, Arizona 85034
Attn: Librarian

Jet Propulsion Laboratory
California Institute of Technology
3800 Oak Grove Drive
Pasadena, California 91103
Attn: Lance Hays

Lawrence Radiation Laboratory
P. O. Box 808
Livermore, California 94550
Attn: Dr. James Hadley - 2 copies

Massachusetts Institute of Technology
Engineering Projects Laboratory
Research Laboratory of Electronics
Cambridge, Massachusetts 02139
Attn: Prof. George A. Brown

Mechanical Technology Incorporated
968 Albany-Shaker Road
Latham, New York 12110
Attn: Dr. Beno Sternlicht

National Bureau of Standards
Washington, D. C. 20225
Attn: C. W. Beckett

Power Information Center
University of Pennsylvania
3401 Market Street, Room 2107
Philadelphia, Pennsylvania 19104

Pratt and Whitney Aircraft
United Aircraft Corporation
East Hartford, Connecticut 06108
Attn: Dr. W. Lueckel

Pratt and Whitney Aircraft
United Aircraft Corporation
East Hartford, Connecticut 06108
Attn: W. H. Podelny

Southwest Research Institute
8500 Culebra Road
San Antonio, Texas 78206
Attn: Dr. R. A. Burton

Sundstand Aviation-Denver
Division of Sundstrand Corporation
Denver, Colorado 80221
Attn: Robert Boyer

TRW Incorporated
TRW-Electromechanical Division
7209 Platt Avenue
Cleveland, Ohio 44104
Attn: Frank Bayer

TRW Incorporated
TRW-Equipment Laboratory
23555 Euclid Avenue
Cleveland, Ohio 44117
Attn: J. E. Taylor

Westinghouse Electric Corporation
Astronuclear Laboratory
Box 10864
Pittsburgh, Pennsylvania 15236
Attn: R. T. Begley

Westinghouse Electric Corporation
Astronuclear Laboratory
Box 10864
Pittsburgh, Pennsylvania 15236
Attn: W. D. Pouchot

Distribution List For Final Report - Contract NAS 3-8520

Westinghouse Electric Corporation
Research Laboratories
Pittsburgh, Pennsylvania 15236
Attn: J. Boyd

Aeronautical Systems Division
Aeromechanical Branch
Wright-Patterson AFB, Ohio 45433
Attn: Charles Armbruster
       ASRMFP-1

Aeronautical Systems Division
Wright-Patterson AFB, Ohio 45433
Attn: George Sherman API

Aeronautical Systems Division
Wright-Patterson AFB, Ohio 45433
Attn: George E. Thompson APIP-1

Aerospace Research Laboratory
Building 450
Wright-Patterson AFB, Ohio 45433
Attn: Dr. G. Gyarmathy ARN

Oak Ridge National Laboratory
P. O. Box X
Oak Ridge, Tennessee 37831
Attn: William O. Harms
       Metals & Ceramics Division

Oak Ridge National Laboratory
P. O. Box Y
Oak Ridge, Tennessee 37831
Attn: H. W. Savage

Oak Ridge National Laboratory
P. O. Box Y
Oak Ridge, Tennessee 37831
Attn: Dr. Arthur Fraas